Elevation dependent precipitation and temperature changes over Indian Himalayan region

A. P. Dimri[!,@], E. Palazzi[#] and A. S. Daloz[$]

[!]School of Environmental Sciences, Jawaharlal Nehru University, New Delhi, India

[#]Institute of Atmospheric Sciences and Climate, National Research Council, Torino, Italy

[$]Center for International Climate Research, Oslo, Norway

[@]Address for correspondence: Prof. A. P. Dimri, School of Environmental Sciences, Jawaharlal Nehru University, New Delhi, India, 110067. Email: apdimri@hotmail.com

Abstract

Various studies reported an elevation dependent precipitation and temperature changes in mountainous regions of the world including the Himalayas. Various mechanisms are proposed to link the possible dependence of the precipitation and temperature on elevation with other variables, including, long- and short-wave radiation, albedo, clouds, humidity, etc. In the present study changes and trends of precipitation and temperature at different elevation ranges in the Indian Himalayan Region (IHR) is assessed. Observations and modelling fields during the period 1970-2099 are used. Modelling simulations from the Coordinated Regional Climate Downscaling Experiment - South Asia experiments (CORDEX-SA) suites are considered. In addition, four seasons - winter (Dec, Jan, Feb: DJF), pre-monsoon (Mar, Apr, May: MAM), monsoon (Jun, Jul, Aug, Sep: JJAS) and post-monsoon (Oct, Nov: ON) – are considered to detect the possible seasonal response of elevation dependency. Firstly, precipitation and temperature fields, separately, as well as the diurnal temperature range (DTR) are assessed. Following, their long-term trends are investigated, if varying, at different elevational ranges in the IHR. To explain plausible physical mechanisms due to elevation dependency, trend of other variables viz., surface downward longwave radiation (DLR), total cloud faction, soil moisture, near surface specific humidity, surface snow melt and surface albedo, etc. are investigated. Results point towards an decreased (increased) precipitation in higher (lower) elevation. And amplified warming signals at higher elevations (above 3000 m), both in daytime and nighttime temperatures, during all seasons except the monsoon, are noticed. Increased DLR trends at higher elevation are also simulated well by the model and are likely the main elevation dependent driver in the IHR.

Keywords: Indian Himalayan Region, elevation dependent warming, elevation dependent precipitation change, snow-albedo feedback, downward longwave radiation, snow melt, cloud feedback

1. Introduction

Mountain regions are among the most vulnerable areas to climate change and to its impacts both in high-altitude environments and in their surroundings (HIMAP, 2019). In this regard, Messreli and Ives (1997) highlighted the major implications of changing climate on sustainable development in mountains with an interdisciplinary approach where questions concerning mountain culture, water resources, energy, biodiversity, environmental and socio-economic issues are documented. Barry (1992) discussed the amplified amplitude of climate variability and change at various scales in several mountainous regions across the globe and assessed the limitations arising from the paucity and sparseness of observations and lack of theoretical understanding of some physical processes shaping mountain climate and variability.

Indian Himalayan region (IHR) orography controls and/or modulated the precipitation patterns and its elevation dependant distribution. Its topography, a physical barrier, interacts and modulates the weather which flows and controls elevation/vertical precipitation distribution and atmosphere as well (Dimri, 2004; Anders et al., 2006; Dimri, 2009; Dimri and Niyogi, 2012;

Ghimire et al., 2018). Due to which elevation dependent estimation of precipitation, solid-liquid amount ratio, over the IHR remains a major challenge (Palazzi et al., 2013). IHR receives precipitation during winter (Dec, Jan, Feb: DJF) due to western disturbances (WDs; Dimri, 2004; Dimri et al., 2015) and during summer (Jun, Jul, Aug, Sep: JJAS) due to Indian summer monsoon (ISM) (Mathison et al., 2013; Kulkarni et al., 2013). ISM brings almost 80% precipitation in eastern and central part of IHR (Fasullo and Webster, 2003) and roughly 20% over the western part including northern Pakistan and Afghanistan (Singh et al., 2011). The WDs yields most the winter precipitation over western part of the IHR (Dimri and Mohanty, 2009; Rajbhandari et al., 2014). Kulkarni et al. (2013) and Kumar et al. (2015) have stated that due to lack of proper network stations and paucity of observations, understanding of precipitation distribution in IHR and in particular its elevation distribution is limited. Due to the recent climate change impacts and debates thereon, elevation dependent drying and/or wetting is important to assess.

Using station observations over various mountain ranges, Diaz and Bradley (1997) provided a comprehensive survey of elevation dependent temperature changes and found strong evidences of high altitude warming in parts of Asian and European high-altitude regions. Liu and Chen (2000) found a significant amplification of warming rates with elevation, analysing temporal trends of temperature measured at 197 in-situ stations at various elevations over the Tibetan Plateau. Thompson et al. (2003) showed elevation dependency in millennium scale temperature trends for Tibet. Similar studies over the Alps (Giorgi et al., 1997) and the Rocky Mountains (Fyfe and Flato, 1999; Snyder et al., 2002) were carried out, highlighting the existence of differential warming with elevation. The observational studies, however, do not provide an unambiguous picture of elevation dependent warming (EDW): while many of them point towards a positive EDW, others show a decrease of warming rates with elevations and still others found very complex patterns of warming with elevation, including cases in which there is no significant dependence at all (refer Pepin et al., 2015 for a comprehensive review on the topic). For example, in a study based on 1000 high elevation stations across the globe, Pepin and Lundquist (2007) found no significant relationships between warming rates and elevation but found strongest warming trend near the zero degree isotherm, which was attributed to the key role of the snow-ice/albedo feedback.Further, Pepin et al. (2019) have shown limited EDW in the Qilian mountains.

Rangwala et al. (2009) studied the influence of changes in surface specific humidity on downwelling longwave radiation (DLR) which is responsible for pronounced warming during winter over higher altitudes in Tibetan Plateau. In their study based on the analysis of high altitude station data in the Alps, Ruckstuhl et al. (2007) detected an EDW signal and found a correlation with enhanced DLR at higher elevations, owing to the increased DLR sensitivity to surface water vapour increase. Liu et al. (2009) reported elevation dependent temperature changes over most mountain ranges across the globe, including the Tibetan Plateau. They analysed both instrumental data and model simulations in different elevation zones and found that during winter and spring, warming is more pronounced at higher elevations and this was found both in the past and in future projections. Using satellite data from the Moderate Resolution Imaging Spectrometer (MODIS), Qin at al. (2009) found higher warming in the range of 2000-4800 m with respect to lower and higher elevations in Tibetan Plateau. Gao et al. (2019 and 2021) have shown dampened EDW over and beyond 4500m and regional warming is main controlling factor for EDW in Tibetan Plateau. In a study carried out over ten major mountain ranges across the world, Ohmura (2012) found temperature variability and trend to increase with elevation and found a link between EDW and diabatic processes in the middle to high troposphere as a result of cloud condensation. Rangwala and Miller (2012) provided a comprehensive review of EDW globally (refer their Table 1) and identified four main driving mechanisms related to (1) snow-ice/albedo feedback, (2) cloud cover, (3) water vapour modulation of longwave heating and (4) aerosol impact.

Further, using a 1-D radiative transfer model, Rangwala (2013) showed the possibility of strong modulation of surface DLR caused by increase in atmospheric moisture in higher altitudes (>3000 m) during winter which is responsible for amplified warming at higher elevations during winter. Global and regional climate models have been widely used to better understand elevation dependency and specially to explore its possible driving mechanisms and involved feedbacks, both at the global and regional scale. Based on the Climate Model Intercomparison Project phase 5 (CMIP5) global climate models (GCMs), Rangwala et al. (2016) showed that amplified warming during winter in higher elevation regions of northern hemisphere midlatitudes is strongly correlated with elevation dependent increase in water vapour and its modulation of longwave radiation. In another model-based study, Palazzi et al. (2019) used an individual GCM simulation at different resolutions (from about 125 km to about 16 km) and found that the most significant drivers of EDW in the Rocky Mountains, the Himalayas and the Alps are the changes in surface albedo and in DLR. However, the same study shows that over the IHR an additional key driver is the change in surface specific humidity with elevation.

The IHR is identified as one climate and climate change hotspot, since climate change and its impacts on, among others, the cryosphere, biodiversity and water resources are amplified. Among the factors which still hamper the detection and understanding of elevation dependent changes in precipitation and temperature is the paucity of the observations especially at the higher elevations. This is particularly true for the IHR, which plays a crucial role in defining hydro-climatic regimes of the Indian sub-continent. Debate on disappearing glaciers (Tobias et al., 2012), changes in snow depth and cover, permafrost thawing, upslope shift of snowline and treelines in this region is looming large as it can have significant consequences for the hundreds of millions of people living in the Indian sub-continent.

Therefore, this paper examines the existence and mechanisms of elevation dependant precipitation and temperature changes in the IHR, using climate model simulations performed with the state-of-the-art RCMs for both historical and future conditions, overall covering the period 1970-2099 from Coordinated Regional Climate Downscaling Experiment - South Asia experiments (CORDEX-SA) initiative (Giorgi et al., 2009).

The paper is structured as follows: Section 2 describes the study area, the employed model data and the methods used for analysis; Section 3 describes the results on seasonal precipitation and its elevation distributions and changes in present and future. Further, seasonal elevation dependant temperatures and other variables, with the aim of identifying possible driving mechanisms of the dependence of warming rates on elevation is discussed. Section 4 provides mechanism of elevation dependent temperature changes. Finally, Section 5 provides salient findings of the paper under conclusions.

2. Study Area, Data and Methods

2.1. Study Area

The study area considered for this work, shown in Fig. 1a and 1b, includes the entire stretch of southern rim of the Himalayas (hereafter referred to as Indian Himalayan Range, IHR). We chose an area similar to that analysed in recent model based studies (e.g., Ghimire et al., 2015;

Nengker et al., 2017; Choudhary and Dimri, 2017; and others), which has allowed to compare our results with those already found in the literature.

2.2. Data and Methods

In order to assess present and future characteristics and drivers of elevation dependency of precipitation and temperature over IHR we analysed the available observations, Asian Precipitation—Highly Resolved Observational Data Integration Towards Evaluation of Water Resources (APHRODITE, Yatagai et al., 2012) for precipitation and Asian temperature from APHRODITE (APHROTEMP) for temperature. It is having horizontal resolution of 0.44° lat/lon, which is in correspondence to the simulated precipitation fields from the regional climate models (RCMs; refer Table 1 of Ghimire et al., 2015) performed within the framework of the Coordinated Regional Climate Downscaling Experiment-South Asia (CORDEX-SA). The necessary large-scale forcing to these RCMs is provided by global climate model (GCM) simulations. CORDEX-SA is the South Asian component of the CORDEX regional climate modeling initiative (Giorgi et al., 2009; Lake et al., 2017) coordinated by the World Climate Research Programme (WCRP). The horizontal resolution of the model simulations is 0.44° lat/lon. *For further information on the model configuration and experimental design refer to Ghimire et al. (2016) and Nengker et al. (2017) where the model skills in simulating the precipitation and temperature spatial distribution are discussed in detail.* Kumar et al. (2013) discussed the representation of topography in the model. Model simulations from 1970 to 2099 are considered under “present” (1970 -2005), “near future” (2020 -2049) and “projection” (2006-2099) time slices. Future forcings under different representative concentration pathway scenarios (RCPs) are considered as well. These emission pathways represent the trajectory of achieving the least greenhouse gas concentration levels in future through a stringent climate mitigation policy

(Van Vuuren et al., 2006, 2011) and was founded by the modeling team IMAGE from the Environmental Assessment Agency of Netherlands. We decided to use the available scenarios to analyse the response over the IHR, which is considered to be one of the most important climate hot-spot regions, to the most conservative of all emission scenarios.

3. Results and discussion

First, the present climatology and linear trend of precipitation and temperature with elevation distribution; followed by near future monsoon (Jun, Jul, Aug, Sep: JJAS) and winter (Dec, Jan, Feb: DJF) precipitation changes and its annual spatially averaged precipitation distribution is discussed. Different altitude bins at 1000 m interval in the IHR is examined for identifying possible signals of elevation dependency. With this aim, we considered different elevation ranges at 1000 m (or bands) and calculated average of each variable over the grid cells within these elevation range. Then discussion about maximum and minimum temperature, diurnal temperature range (DTR) is carried out. This analysis is performed separately for four seasons - winter (Dec, Jan, Feb: DJF), pre-monsoon (Mar, Apr, May: MAM), monsoon (Jun, Jul, Aug, Sep: JJAS) and post-monsoon (Oct, Nov: ON) - to assess the seasonal response of elevation dependency. Following, identification of the possible elevation dependency drivers, long-term trends in other variables is carried out. The considered variables are downward longwave radiation (DLR), total cloud faction, soil moisture, near surface specific humidity, surface snow melt and surface albedo.

In the succeding sections, we first discussed the elevation dependency of the precipitation, its trend and change in near future; followed by temperatures and their trends. In later sections, detailed discussion on elevation dependency of various atmospheric variables and their trends is presented.

3.1. Precipitation

Precipitation distribution over the elevations in IHR (Fig. 1b) is very complex and non-linear in nature. This is primarily led by the precipitation forming mechanism and orographic controls over the region (though not discussed in the present manuscript, refer Ghimire et al., 2015). Fig. S1a (blue color on right hand side) depicts the observed annual averaged precipitation during present (1970 – 2005) over the IHR. Fig. S1(aa-ak) represent model biases and Fig. S1(al) represents ensemble bias with the corresponding observation (Fig. S1a blue color on the right hand side). Simulated precipitation spatial distribution based on CORDEX-SA 11 RCM members (Fig. S1aa-ak) and their ensemble (Fig. S1al) is presented here. Most of the models have wet (dry) bias over the higher elevation (lower elevation and foothill) of the Himalayas. There is distinct transition in precipitation in models' environment as we move across the Himalayas from lower to higher elevations. Model environment is drier in lower elevation and as we move towards higher elevation it gets wetter. These could be attributed primarily due to precipitation forming processes with in the model physics and model topography representation. Fig. S1b (right hand side) represent precipitation distribution in vertical elevation in the IHR. It could be seen that in lower elevation(s) precipitation is widely spread and distributed which at the higher elevation is closely clustered around. In mid-elevation is it scattered around with no definite patterns. Mid-elevation seems to have a certain kind of threshold where above and below precipitation mechanisms are differed and which is reflected thus in Fig. S1a. Further, Fig. S1(ba - bk) and Fig. S1bl shows the difference of elevation precipitation distribution in models and their ensemble from their corresponding observation (Fig. S1b right hand side). In most of the models lesser (higher) precipitation in lower (higher) elevations is seen. Here, again, in and around mid-elevations undefined/unstructured difference in precipitation is noticed. For assessing this better, variability and trends in elevation dependent precipitation in observation is shown in Fig. S1c. Here it is clearly seen that precipitation has higher (lower) variability in and around lower (higher) elevation. And there is transition of this pattern in and around mid-elevation. In addition, there is change in trends in and around mid-elevation: according to which higher (lower) elevations are having increased (decreased) precipitation trends. Overall, it illustrates that in different elevation ranges lower elevations have more diverse but higher precipitation; mid-elevation have not so diverse but scattered precipitation and upper elevation have more concentrated but lesser precipitation. It indicates that there is kind of threshold in and around mid-elevation where precipitation distribution gets changed above and below it. Higher, though diverse, precipitation in lower elevations and lower, though concentrated, precipitation in higher elevations is a reflection of associated precipitation forming mechanisms. However, scattered mid-elevation precipitation still remains 'an intriguing research question'. In case of statistically significant change in precipitation trend during present it is seen that precipitation decreases in lower elevation up to mid-elevation and increases above it. Here we also see that lower (higher) elevation has higher (lower) precipitation variabilities which decreases from lower to higher elevation. It also justifies that mid-elevation acts as a threshold where precipitation mechanism and change reverses.

Near future (2020 – 2049) projection of spatial monsoon (JJAS) precipitation distribution based using suitable 08 RCM members from CORDEX-SA experiment (Fig. 2aa-ah) and their ensemble (Fig. 2ai) in RCP8.5 is presented. It illustrates precipitation change during near future (2020 – 2049) from the present (1970 – 2005) in percentage. It shows a dipolar pattern change as eastern (western) Himalayas will receive decreased (increased) precipitation in near future. It should as well be noted that there are high uncertainty among models in itself (discourse and discussion on CORDEX-SA model and related information is not provided due to brevity of the volume, please refer Choudhary and Dimri, 2017). Further, elevation dependent distribution of difference (near future minus present) in precipitation trends during winter, Fig. 2b(a-c), and monsoon, Fig. 2b(d-f), based on 10 RCM members and their ensemble in RCPs 2.6, 4.5 and 8.5 respectively is presented and investigated. Overall, it indicates that lower elevations show increased variability in future with increased precipitation as well. This feature gets prominent in near future under RCP8.5, in particular. In addition, increased uncertainty at higher elevations, though less than lower elevations, is seen as well. Lesser variability in higher elevations could be due to the reason that higher elevations receive scanty precipitation. However, ensemble precipitation shows increased precipitation in near future than present.

Further, spatially averaged monsoonal precipitation over the IHR from 1970-2099 is shown in Fig. 3. It is based on 08 RCM members and their ensemble in RCP2.6, 4.5 and 8.5 as Fig. 3a, 3b and 3c respectively. Long term average in RCP2.6 has less variabilities. Higher errors and/or variabilities in future trends of model precipitation fields are seen in RCPs 4.5 and 8.5. However, it is interesting to note that ensemble averaged monsoonal precipitation based on these model show similar, but increasing, trends in all the three RCPs. Figures depict the increased monsoonal precipitation in the future time lines but with certain uncertainty. Comparison with present (1970 - 2005) spatially averaged annual precipitation shows that models are wet biased but show the similar variability as in the corresponding observations.

3.2. 2m Temperature

Similarly, here temperature field is discussed. Fig. S2(a) represents temperature biases in winter (DJF: left most column), pre-monsoon (MAM: left middle column), monsoon (JJAS: right middle column) and post-monsoon (ON: right most column) in five of the best models of

CORDEX-SA experiment and their ensemble during present (1970 – 2005). In most of the model distributions, higher (lower) elevations comparatively show colder (cold) biases. In addition, model higher elevations are colder than the lower elevations. It indicates that elevation depended temperature decreases are rapid in model. Few of the models show warm biases, but limited within lower elevations, along the foothill of the IHR during MAM. MAM is the time when temperature started rising in the northern latitudes of the IHR. Ensemble biases provide a mean picture out of these models and reaffirm that models are colder (cold) over the higher (lower) elevations than the corresponding observations. Corresponding elevation dependent scatter distribution of grid temperature averaged during winter (DJF; Fig. S2ba), pre-monsoon (MAM; Fig 4bb), monsoon (JJAS; Fig. S2bc) and post-monsoon (ON; Fig. S2bd) is presented. Decrease of temperature with elevation is seen, but there are grid scale variability. At higher elevation more variability than the lower elevation is seen. It is to do with slope environmental lapse rate than the vertical atmospheric lapse rate (Thayyen and Dimri, 2019). Further percentage differences in near future (2020 – 2049) from present (1970 – 2005) in five models and their ensemble are presented during winter (DJF: left most column), pre-monsoon (MAM: left middle column), monsoon (JJAS: right middle column) and post-monsoon (ON: right most column) in Fig. S2c. Percentage change in near future illustrates more variability in elevation dependent temperature distribution. Lesser is the variability in lower elevations and as we move towards higher elevation in expands, though over all there is decrease in temperature with elevations in models and their ensemble. To understand these issues, statistical features in models and their ensemble with their corresponding observation is estimated and presented in Fig. S2d during winter (DJF; Fig. S2da); pre-monsoon (MAM: Fig. S2db); monsoon (JJAS: Fig. S2dc) and post-monsoon (ON: Fig. S2dd). Probability distribution functions of temperature distribution during present (1970 – 2005) are presented and it is seen that in all the seasons models and their ensemble mean correspond to lower values than their corresponding observation. In addition, two important features, first, their shifting towards left and, second, higher spread too are noticed. Lower mean corresponds to the cold bias in models and more spread corresponds to higher variability.

3.3. Mean, maximum and minimum temperature and comparison with their corresponding observation (duirng present)

The mean temperature spatially averaged over the study region in the model simulation under RCP8.5 scenario from 1970 - 2099 along with present (1970-2005 from the APHROTEMP dataset) during winter (DJF; Fig. 4a); pre-monsoon (MAM: Fig. 4b); monsoon (JJAS: Fig. 4c) and post-monsoon (ON: Fig. 4d) is presented. In top left corner of each figure spatially averaged present mean temperature is also presented. These trends are statistical significant as described in figure. In all the seasons increased mean temperatures are seen over the years. Distinct increase in models ensemble too is seen. In addition, larger variability are seen in the model fields. Increased variability in mean temperature values are seen during far future than near future. Warming rates are higher during winter and post-monsoon. Due to moisture, dampening in temperature variability is seen during monsoon. However overall increase in temperature values in all the four seasons is discernible.

Similar statistically significant trends in maximum and minimum temperatures spatially averaged over the study region in the model simulation under RCP8.5 scenario from 1970 - 2099 along with present (1970-2005 from the APHROTEMP dataset) are shown in Fig. 5 and 6 during winter (DJF; Fig. a); pre-monsoon (MAM: Fig. b); monsoon (JJAS: Fig. c) and post-monsoon (ON: Fig. d) respectively. Minimum temperature (Fig. 6) in all the seasons show more variabilities than maximum temperature (Fig. 5). Highest variability during winter is found in minimum temperature, which in case of maximum temperatures is during monsoon. Here too, in monsoon increase of temperatures are dampened as compared to other seasons.

Further seasonal grid averaged elevation dependent distribution of difference in mean temperature trends in near future (2020 – 2049) in RCP8.5 scenario from present (1970-2005 from the APHROTEMP dataset) is shown in Fig. 7 during winter (DJF; Fig. a); pre-monsoon (MAM: Fig. b); monsoon (JJAS: Fig. c) and post-monsoon (ON: Fig. d) respectively . Figure depicts higher (lower) warming rates in higher (lower) elevations. They are more pronounced during post-monsoon than other seasons. These analyses are presented from two models: REMO and SMHI only which come within +/- 1 std. dev. of present (1970-2005 from the APHROTEMP dataset).

3.4. Trends in mean, maximum and minimum temperature and their diurnal temperature range

The maximum and minimum temperature trends as a function of the elevation are shown in Fig. 8 and 9, respectively, for the different seasons (panels a-d). During winter, the maximum temperature trend (Fig. 8a) exhibits a slight decrease with elevation from the surface up to ~ 2000 m and then it increases from ~ 3500 m upward. At intermediate elevations, between about 2000 and 3500 m, no significant variation with elevation is found except a slight increase around 2500 m a.s.l. In minimum temperature trend (Fig. 9a) overall increase with elevation from the surface upward is seen, though they are not similar everywhere. In the pre-monsoon, the maximum temperature (Fig. 8b) shows a negative trend from the surface up to ~ 1500 m and above 5000, while a positive trend is found between about 1500 and 5000 m a.s.l. The minimum temperature trend, shown in Fig. 9b, has a similar behaviour as the maximum temperature trend in the pre-monsoon, except above 5000 m where the trend continues to be positive. It indicates that maximum (minimum) temperature is (decreasing) increasing at higher elevation during pre-monsoon. The monsoon is characterized by an almost constant maximum temperature trend (0.011ºC/year) with elevation up to ~ 3000 m and a higher constant value (0.013ºC/year) from about 5000 m upward, while from ~ 3000 to 5000 m the trend is positive (Fig. 8c). In this season, the minimum temperature exhibits an almost constant trend with elevation up to 3000 m a.s.l. and a positive trend 3000 to 4500 m a.s.l.; the trend then decreases above 4500 m a.s.l. (Fig. 9c). During monsoon lower troposphere is comprised of moisture which then retains almost consistent elevation distribution trend up to mid-elevations. Finally, during the post-monsoon the maximum temperature trend (Fig. 8d) increases with the elevation from the surface up to ~ 4500 m, while no significant changes are found above that altitude. Minimum temperature warming rates point towards a positive dependence (Fig. 9d). In summary, trends in maximum and minimum temperature, overall, indicate higher warming rates at higher elevations, though with different elevational patterns depending on the season and on the considered variable (either the minimum or the maximum temperature).

Further, diurnal temperature range (DTR: difference between the maximum and the minimum temperature) trends during period 1970-2099 and their dependence on elevation is analysed. As shown in Fig. 10, DTR trends are negative in every season except in monsoon, which means that the minimum temperatures increase more than the corresponding maximum temperatures. This is often referred to as daily asymmetry in warming rates and has been found in previous studies focused over Tibetan Plateau (e.g., Liu et al., 2009, Palazzi et al., 2016); over Alps (Jungo and Beniston 2001) etc. During winter (panel a), DTR trends are more negative at higher elevations, corresponding to a faster minimum temperature increase with elevation than of the maximum temperature (see also Fig. 8a and 9a). No elevation dependent changes in DTR trends are depicted during the pre-monsoon (Fig. 10b) from the surface up to ~ 3000 m, while a decrease occurs above that elevation. During the monsoon, (see panel 10c), we found near to zero changes in DTR up to 3000 m while positive trends with elevation are observed above. An overall negative elevational gradient of the DTR (negative trend) is observed during post-monsoon (Fig. 10d), similar as of winter..

3.5. Elevation dependent warming (EDW) drivers

In this section, a joint analysis of EDW (in the mean temperature) and altitudinal dependence of the trend in other variables is performed, in order to understand the possible mechanisms responsible in the IHR region.

3.5.1. Winter

Fig. 11 shows winter altitudinal trends, calculated during 1970-2099, of the mean temperature (a), DLR (b), total cloud fraction (c), total soil moisture (d), near surface specific humidity (e), near surface snow melt (f), surface albedo (g) and the ratio between the DLR trend and the near surface specific humidity trend (g) over IHR. As shown in Fig. 11a, warming rates in the mean temperature are amplified with elevation from about 1500 m upwards. Elevational decrease of DLR trend below ~3000 m and increases above it is seen, Fig. 11a. This increase leads to enhanced surface heat storage at these elevations, which has been recognized as one primary mechanism responsible for high altitude warming in this and other mountains in the northern hemisphere mid-latitudes (e.g., Rangwala et al., 2009, 2010, 2016; Rangwala, 2013; Ruckstuhl, 2007, Palazzi et al., 2017, 2019). Fig. 11c shows that the total cloud fraction trend is negative, indicating a decrease of cloud cover over time, and that this decrease is amplified with elevation up to about 3000 m, while it reduces between about 3000 and 5000 m. The total soil moisture

(Fig. 11d) is characterized by a negative trend which, however, becomes less negative with elevation until about 2000 m where it stabilizes around zero, i.e., total soil moisture does not exhibit any trend from about 2000 m upwards. Near surface specific humidity trend (Fig. 11e) is positive but its elevational gradient is negative. It indicated that the specific humidity trend is likely have lesser increase in the future over higher elevations compared to lower elevations. Previous studies have shown that, particularly during winter, large deviations in DLR are linked to deviations in atmospheric moisture content. The sensitivity of DLR changes to changes in atmospheric moisture increases at low atmospheric moisture values (typically < 2.5g/kg; Rangwala et al., 2009). These conditions exist during winters in dry environments, like those encountered in high elevation areas. Further, altitudinal decrease in humidity trends depicts increased convective loss of moisture. It will lead to increase sensible heat flux and enhancement of mean temperature. Elevational variations of the surface snow melt trend (Fig. 11f) and of the albedo trend (Fig. 11g) are closely related, as expected. The snow melt peak occurs around an elevation (about 3000 m) where the albedo trend is most negative, indeed. The change in snow melt (albedo) rate- decrease (increase) - above 3000 m would dampen the positive DLR-moisture feedback resulting surface heating. This feedback is significant for EDW as the ratio - between the rate of changes of DLR and near surface specific humidity - increases with elevation, Fig. 11h. Hence, in higher elevations, an enhanced DLR with a certain increase in moisture dominates as compared with lower elevations. In lower elevations sensitivity of DLR to moisture content is less pronounced. This mechanism becomes more critical during winter when the moisture content is lower than a critical threshold. Further, the total cloud fraction change would control DLR as well leading to increase over higher elevation. Increased daytime cloud cover would reduce surface insolation leading to decreased temperature. It will counter the DLR-moisture feedback and dampen the EDW. In winter, a distinct kink at ~ 3500 m partitioning trend reversal in most of the variables is seen. It illustrates an altitude threshold, beyond and below which the EDW and associated mechanism reverses. However, over IHR, in winter (monsoon) most of the cloud formations are due to orographic lifting or frontal mechanism (convection as well) which form mainly at mid-level.

3.5.2. Pre-monsoon

A slight decreasing (increasing) trend of mean temperature at lower (upper) elevation is seen in the pre-monsoon (Fig. 12a) while DLR trends, shown Fig. 12b, decrease with elevation throughout the entire altitude range. Higher elevation atmospheric dryness and stability leads to such processes. Altitudinal trend of the total cloud fraction is found which is characterized by almost constant values until about 3000 m. Above it and up to 5000 m a sudden reduction in its values and then again steady values above it is seen (Fig. 12c). Interestingly, the trends of total cloud fraction are constant below 3000 m (indicating consistent total cloud fraction with time) and negative above 5000 m. The cloud fraction trend reduction with elevation between about 3000 m and 5000 m would enhance absorbed solar radiation at the surface. It will lead to increased snow melt (Fig. 12f) which will allow solar radiation absorption and more heat storage at the higher elevations (Yan et al., 2016). Total soil moisture trend with increased elevation does not significantly change, Fig. 12d. Decrease in near surface specific humidity trends with elevation are seen (see Fig. 12e). It is seen similar to the winter time though the rates are difference. The snow melt trends shown in Fig. 12f reflect similar trends as of surface albedo (Fig. 12g). Due to decreased surface albedo/snow, increased surface absorption of solar radiation occurs in particular during summer at higher elevations in association with the 0°C isotherm (Pepin and Lundquist, 2008). This can contribute to enhanced temperature trends. The ratio between DLR trends and near surface specific humidity trends (Fig. 12h), though increases from lower to higher elevations but remains stable in and around mid-elevation.

3.5.3. Monsoon

The mean temperature trend slightly decreases with elevation (Fig. 13a). Elevational decrease in DLR trend up to 3000 m, then increase from about 3000 m to 4000 m and then decrease above is seen (Fig. 13b). Almost specular total cloud fraction trends with elevation are found (Fig. 13c). During monsoon, increased moisture in the free atmosphere plays a role for cloud formation. An increased daytime cloud cover decreases the amount of solar radiation reaching the ground, which strongly influences mean temperature and determine the reduced trends during the monsoon. The cloud fraction trend increases with elevation causing increased availability of moisture thus enhancing the DLR. During this season, differing with the situation encountered in winter, the moisture content is likely beyond the threshold (2.5 g/kg; Rangwala et al., 2009) to which DLR is sensitive due to specific humidity variations. Further, total soil moisture trends as well does not change with elevation, Fig. 13d. Near surface specific humidity trends decrease with elevation, Fig. 13e, a behaviour common to all seasons. Higher elevations will retain snow longer as snow melt trends are decrease as compared to lower elevations, Fig. 13f. Corresponding trends in surface albedo decrease with elevations, Fig. 13g. The increased surface absorption of solar radiation is an important mechanism as higher elevations show smaller trends than lower elevations. Trends of ratio - of DLR to the near surface specific humidity trends - show variable trends but with a general increase with elevation, Fig. 13h.

3.5.4. Post-monsoon

During post-monsoon, mean temperature trend does not change up to 2000 m elevations. Interestingly, within 2000 -3500 m, it first increases and then decrease and follows a curvilinear path. Beyond 4000 m it increases again (Fig. 14a). It is seen that after winter, post-monsoon shows strongest signal of EDW as reported in other studies too (e.g., Liu et al., 2006; Rangwala et al., 2009). DLR reflects similar distribution as of altitudinal temperature changes (Fig. 14b) with increasing trend beyond 3500 m. In mid elevation regions, initially increasing and the decreasing trends are seen. DLR trends do not significantly changing in lower elevation. Distinct cloud fraction trends increase between 3500-5000 m is seen. It illustrates linkages with increased DLR on surface, Fig. 14c. Total soil moisture trends decrease faster in lower elevations than in upper elevations, Fig. 14d. This decrease implies a reduction (increase) in latent (sensible) heat fluxes. Such changes will strongly affect to the surface snowmelt. Consistent decreasing near surface humidity trends with elevation is observed. Thus, due to convective loss of moisture by near surface heating will lead to a higher sensible heat flux, Fig. 14e. In case of surface snow melt, upper elevations indicate higher snow melt then the lower elevations, Fig. 14f. These trends are similar to ones of surface albedo trends, Fig. 14g. Ratio of trends DLR to near specific humidity, it increases with elevations, Fig. 14h.

4. EDW Mechanisms

This study shows amplified warming with elevation during all seasons, except the monsoon, in the IHR. Mid-elevations act as threshold over which temperature trends have non-similar responses. Among many possible mechanism leading to enhanced warming in higher elevations there are several feedbacks in mountains regional climate systems viz. snow-albedo feedback (Giorgi et al., 1997; Fyfe and Flato, 1999; Rangwala et al., 2010); the cloud-radiation feedback (Liu et al., 2009); the feedback related to humidity and DLR (Rangwala et al., 2009; Rangwala, 2013; Naud et al., 2013); etc. All these proposed feedbacks are linked with reasons and causes associated with number of variables viz., soil moisture (Liu et al., 2009, Naud et al., 2013);

aerosols (Lau et al., 2010); clouds and their coverage (Sun et al., 2000); etc. These interlinking variables and processes change and contribute to surface energy balance, in particular within the context of EDW.

In the present study, we found that enhanced increased DLR fluxes at higher elevations of the IHR is primarily responsible for warming amplification, in particular during winter. Possible coupling of mountainous surface processes with atmosphere feedbacks determine magnitude and pattern of DLR variations. It characterizes elevation dependent amplification as we move from lower to higher elevations and above a certain threshold elevation as well. Near surface humidity is the primary feedback which is responsible for higher DLR trend at higher elevations. DLR-humidity feedback mechanism is one of the most significant drivers in IHR. In addition, snow melt change- surface albedo change beyond 3000 m feedback inhibits the DLR-humidity positive feedback effect on surface heating. Apart from these, some counteracting mechanisms too exist. Cloud fraction trend reduction above and beyond 3000 m lead to enhanced solar absorption at the surface. It will further increase snow melt; decrease in snow depth and reduced surface albedo. It will allow the absorption of solar radiation at higher elevations leading to enhanced surface warming (Yan et al., 2016). In a way this later mechanism will couple with each other.

The longwave radiation sensitivity to surface air humidity increases with elevation till a certain altitude threshold (3000 m) corroborating findings by Ruckstuhl et al. (2007). In which DLR changes are sensitive to specific humidity changes and follow a non-linear relationship and is higher when humidity is lower. It typically exists at high elevations during winter. Increased DLR at higher elevations or at least above the threshold plays significant role in EDW through coupled feedbacks of moisture, cloud and snow cover with radiation.

In the context of moisture or precipitation elevation distribution and its feedback with corresponding temperature elevation distribution - lower elevations receive higher precipitation than higher elevations (see Fig. 6, Palazzi et al., 2014; Ghimire et al., 2015). It view of this higher elevation are comparatively dried than lower elevations. Such higher availability of moisture or precipitation distribution in lower elevation than higher elevation will dampen the temperature warming at lower elevations than at higher elevations. However, it will be seen in details as moisture- temperature feedback in future study.

5. Mechanisms of temperature controls

Amplified warming in 2m maximum and minimum temperature during all seasons, except the monsoon, over most of the elevations, in particular over higher elevations is seen. Mid-elevations act as threshold over which temperature trends have assimilar responses. Previous studies showed that among the possible mechanisms behind amplified warming at higher elevations are several feedbacks acting in the climate system like snow-albedo (Giorgi et al., 1997; Fyfe and Flato, 1999; Rangwala et al., 2010); cloud-radiation (Liu et al., 2009); humidity-DLR (Rangwala et al., 2009; Rangwala, 2013; Naud et al., 2013) feedbacks. These are associated with changes in a number of relevant variables such as soil moisture (Liu et al., 2009, Naud et al., 2013), aerosols (Lau et al., 2010), clouds and their coverage (Sun et al., 2000). These all contribute to variations in the surface energy balance at various scales. In the present study, a high resolution long-term climate simulation of climate over IHR was analyzed to study elevation dependent distribution and its mechanisms over the area. Results indicate that enhanced increase in DLR flux at the higher elevation surface during winter is primarily responsible for high altitude warming amplification. Possible coupling between multiple land-atmosphere feedbacks could explain the magnitude and peculiar pattern of DLR variation during this season characterized by trend amplification above a certain altitude. The primary feedback which is responsible for higher trend of DLR beyond a certain altitude is the humidity- surface DLR feedback which is a significant player during winter season. However, the decrease in the rate of change of snow melt and dependent increase in that of surface albedo beyond 3000 m could subdue the DLR-moisture positive feedback effect on surface heating. On the other hand, there are counter acting mechanisms existing to this process. The reduction in cloud fraction trend values above 3000 m favors the enhancement in net solar radiation received at the surface, with further increase in snow melt/decrease in snow depth thus leading to the reduced surface albedo. This further allows the absorption of solar radiation at higher elevations implying more storage of heat at the higher elevation surface and thereby amplifying the temperature (Yan et al., 2016).

Although the increase in DLR with increase in specific humidity occurs globally, the sensitivity of former to latter follows a non-linear relationship (Ruckstuhl et al., 2007; Rangwala and Miller, 2012) and is particularly high when the humidity levels are low which exists typically at high elevations during winter. In other words, the drier the atmosphere, magnified will be the impact of even smaller changes in humidity on the DLR (Ruckstuhl et al., 2007; Rangwala et al., 2010; Naud et al., 2013). Changes in DLR are more sensitive to changes in humidity when the latter is less than 2.5 g/kg i.e., when the atmosphere is dry (Rangwala et al., 2009) a condition which is more prevalent during winter in the elevated regions. Instead, this phenomenon does not occur during summer season since, as background humidity values are already very high, the sensitivity of surface DLR to any further increase of atmospheric moisture is much less (e.g., Ruckstuhl et al., 2007). Also, as shown in the present study the sensitivity of longwave radiation to surface air humidity increases with altitude above a certain threshold (3000 m) corroborating the results found by Ruckstuhl et al. (2007). This means that, the same amount of changes in the surface air humidity will cause higher amount of changes in DLR at higher elevation sites in comparison to the lower elevation locations (Rangwala, 2013). Increased DLR at the surface in higher elevations or above a critical altitude plays significant role in EDW during winter through coupled feedbacks of moisture, cloud and snow cover with radiation.

6. Conclusions

Analysis of precipitation and temperatures along with other meteorological variables brings in very interesting observations in case of elevation dependant drivers over IHR. Increased precipitation trends in upper elevation as opposite to lower elevation is one of the key suggesting that lower elevations are drying than upper elevations. In addition decreasing (increasing) monsoonal precipitation in near future over eastern (western) Himalayas hints to assess the changing dynamics of Indian summer monsoon.

Lower warming rates in lower elevation is mainly due to presence monsoonal moisture which dampens the warming than over upper elevations. However distinct changes in mid-elevation here are important to note. Higher elevation (> 3000m) shows amplified warming during winter. No distinct change in DTR up to mid-elevation is primarily due to moisture-temperature feedback and increasing trends in upper elevations are due to comparatively drier environment. The surface albedo is calculated as the ratio (in %) of reflected to incident shortwave radiation. Beyond 3000m rate of snow melt tends to decrease with corresponding increase in surface albedo. Further, the elevation dependency of the sensitivity of warming rate to moisture trends is examined looking at the latitudinal distribution of the ratio between the temperature trend and the near-surface specific humidity trend. The pattern is clearly reflected in downwelling longwave radiation (DLR) trend. Increased DLR at higher elevation could be due to various coupled feedbacks: moisture sensitivity and cloud cover increase.

Since the simulation used in this study did not include any aerosol component, the role of this variable in influencing high elevation temperature changes could not be assessed. Incorporating or refining the current representation of aerosol feedbacks in climate models would imply nesting an aerosol component through parametrization of the related forcings or processes. Further, to properly represent the relevant mechanisms and provide a more realistic simulation of the changes in the cryosphere system of high elevation regions an interactive snow/glacier model feedback into a high resolution regional climate model is required. There is also a need for increasing climate monitoring program at high elevation regions with greater number of climatic variables. This will aid in better understanding of present trends and processes that are affecting the state of climate in IHR as well as for validating the model generated information.

Acknowledgements

APD acknowledges financial support by MoEF&CC under NMHS scheme. Authors also acknowledge the Earth System Grid Federation (ESGF) infrastructure and the Climate Data Portal at Centre for Climate Change Research (CCCR), Indian Institute of Tropical Meteorology, India for provision of REMO data under CORDEX-SA.

Declaration

Authors declare that they don't have any conflict in this work.

Data Availability Statement

Data will be provided on request.

References

Barry RG (1992) Mountain climatology and past and potential future changes in Mountain Regions: A Review. Mt Res Dev 12:71–86. doi: 10.2307/3673749.

Beniston M (2003) Climatic change in mountain regions: A review of possible impacts. In: Clim Change 59:5–31. doi: 10.1023/A:1024458411589.

Bolch, T, Kulkarni, A, Kääb, A, Huggel, C, Paul, F, Cogley, JG, Frey, H, Kargel, JS, Fujita, K, Scheel, M, Bajracharya, S (2012) The state and fate of Himalayan glaciers. Science 336:310–314. doi: 10.1126/science.1215828.

Choudhary A, Dimri AP (2017) Assessment of CORDEX-South Asia experiments for monsoonal precipitation over Himalayan region for future climate. Clim. Dyn. 1–22. doi:10.1007/s00382-017-3789-4.

Diaz HF, Bradley RS (1997) Temperature Variations During the Last Century at High Elevation Sites. Climatic Change at High Elevation Sites. 21–47. doi: 10.1007/978-94-015-8905-5_2.

Fyfe, J C and Flato GM (1999) Enhanced Climate Change and Its Detection over the Rocky Mountains. J Clim 12:230–243. doi: 10.1175/1520-0442-12.1.230.

Gao, D, Sun, J, Yang, K, Pepin, N, Xu, Y (2019) Revisiting recent elevation-dependent warming on the Tibetan Plateau using satellite-based data sets. Journal of Geophysical Research: Atmospheres, 124, 15, 8511-8521.

Gao, D, Pepin, N, Yang, K, Sun, J, Li, D (2021) Local changes in snow depth dominate the evolving pattern of elevation-dependent warming on the Tibetan Plateau. Science Bulletin, Volume 66, Issue 11, 15 June 2021, Pages 1146-1150.

Ghimire, S, Choudhary, A, Dimri, AP (2015) Assessment of the performance of CORDEX-South Asia experiments for monsoonal precipitation over the Himalayan region during present climate: part I. Clim. Dyn. 2–4. doi: 10.1007/s00382-015-2747-2.

Giorgetta, MA, Jungclaus, J, Reick, CH, Legutke, S, Bader, J, Böttinger, M, Brovkin, V, Crueger, T, Esch, M, Fieg, K, Glushak, K, (2013) Climate and carbon cycle changes from 1850 to 2100 in MPI-ESM simulations for the Coupled Model Intercomparison Project phase 5. J Adv Model Earth Syst 5:572–597. doi: 10.1002/jame.20038.

Giorgi F, Hurrell JW, Marinucci MR, Beniston M (1997) Elevation dependency of the surface climate change signal: A model study. J Clim 10:288–296. doi: 10.1175/1520-0442(1997)010<0288:EDOTSC>2.0.CO2.

Giorgi F, Jones C, Asrar GR (2009) Addressing climate information needs at the regional level: the CORDEX framework. Bull - World Meteorol Organ 58:175–183. doi: 10.1016/j.jjcc.2009.02.006.

Kumar, P., Wiltshire, A., Mathison, C., Asharaf, S., Ahrens, B., Lucas-Picher, P., ..., and Jacob, D. (2013). Downscaled climate change projections with uncertainty assessment over India using a high resolution multi-model approach. Science of the Total Environment, 468, S18-S30. 10.1016/j.scitotenv.2013.01.051.

Lake I, Gutowski W, Giorgi F, Lee B (2017) CORDEX: Climate research and information for regions. In: Bulletin of the American Meteorological Society. 98:ES189-ES192. doi: 10.1175/BAMS-D-17-0042.1.

Lau WKM, Kim MK, Kim KM, Lee WS (2010) Enhanced surface warming and accelerated snow melt in the Himalayas and Tibetan Plateau induced by absorbing aerosols. Environ Res Lett 5:. doi: 10.1088/1748-9326/5/2/025204.

Liu X, Chen B (2000) Climatic warming in the Tibetan Plateau during recent decades. Int J Climatol 20:1729–1742. doi: 10.1002/1097-0088(20001130)20:14<1729::AID-JOC556>3.0.CO;2-Y.

Liu X, Cheng Z, Yan L, Yin ZY (2009) Elevation dependency of recent and future minimum surface air temperature trends in the Tibetan Plateau and its surroundings. Glob Planet Change 68:164–174. doi: 10.1016/j.gloplacha.2009.03.017.

Liu, X., Yin, Z. Y., Shao, X., and Qin, N. (2006). Temporal trends and variability of daily maximum and minimum, extreme temperature events, and growing season length over the eastern and central Tibetan Plateau during 1961–2003. Journal of Geophysical Research: Atmospheres, 111(D19). doi: 10.1029/2005JD006915.

Messerli B, Viviroli D, Weingartner R (2004) Mountains Vulnerable of the World : Water Towers for the 21st Century. AMBIO Spec Rep 13:29–34. doi: 10.5167/uzh-110516.

Naud CM, Chen Y, Rangwala I, Miller JR (2013) Sensitivity of downward longwave surface radiation to moisture and cloud changes in a high-elevation region. J Geophys Res Atmos 118:10072–10081. doi: 10.1002/jgrd.50644.

Nengker T, Choudhary A, Dimri AP (2017) Assessment of the performance of CORDEX-SA experiments in simulating seasonal mean temperature over the Himalayan region for the present climate: Part I. Clim. Dyn. 1–31. doi:10.1007/s00382-017-3597-x.

Nogués-Bravo D, Araújo MB, Errea MP, Martínez-Rica JP (2007) Exposure of global mountain systems to climate warming during the 21st Century. Glob Environ Chang 17:420–428. doi: 10.1016/j.gloenvcha.2006.11.007.

Ohmura A (2012) Enhanced temperature variability in high-altitude climate change. Theor Appl Climatol 110:499–508. doi: 10.1007/s00704-012-0687-x.

Palazzi, E., Filippi, L. & von Hardenberg, Insights into elevation-dependent warming in the Tibetan Plateau-Himalayas from CMIP5 model simulations, J. Clim Dyn 48: 3991. https://doi.org/10.1007/s00382-016-3316-z, 2017.

Palazzi, E., Mortarini, L., Terzago, S. and von Hardenberg, J., Elevation-dependent warming in global climate model simulations at high spatial resolution, Clim Dyn 52: 2685. https://doi.org/10.1007/s00382-018-4287-z, 2019.

Pepin, N, Deng, H, Zhang, H, Zhang, F, Kang, S, Yao, T (2019) An Examination of Temperature Trends at High Elevations Across the Tibetan Plateau: The Use of MODIS LST to Understand Patterns of Elevation-Dependent Warming. https://doi.org/10.1029/2018JD029798

Pepin N, Bradley RS, Diaz HF, Baraer M, Caceres EB, Forsythe N, Fowler H, Greenwood G, Hashmi MZ, Liu XD, Miller JR, Ning L, Ohmura A, Palazzi E, Rangwala I, Schöner W, Severskiy I, Shahgedanova M, Wang MB, Williamson SN, Yang DQ (2015) Elevation-dependent warming in mountain regions of the world. Nat. Clim. Chang. 5:424–430. doi: 10.1038/nclimate2563.

Pepin NC, Lundquist JD (2008) Temperature trends at high elevations: Patterns across the globe. Geophys Res Lett 35:. doi: 10.1029/2008GL034026.

Qin J, Yang K, Liang S, Guo X (2009) The altitudinal dependence of recent rapid warming over the Tibetan Plateau. Clim. Change doi: 97:321–327. 10.1007/s10584-009-9733-9.

Rangwala I (2013) Amplified water vapour feedback at high altitudes during winter. Int J Climatol 33:897–903. doi: 10.1002/joc.3477.

Rangwala I, Miller JR (2012) Climate change in mountains: A review of elevation-dependent warming and its possible causes. Clim Change 114:527–547. doi: 10.1007/s10584-012-0419-3.

Rangwala I, Miller JR, Russell GL, Xu M (2010) Using a global climate model to evaluate the influences of water vapor, snow cover and atmospheric aerosol on warming in the Tibetan Plateau during the twenty-first century. Clim Dyn 34:859–872. doi: 10.1007/s00382-009-0564-1.

Rangwala I, Miller JR, Xu M (2009) Warming in the Tibetan Plateau: Possible influences of the changes in surface water vapor. Geophys Res Lett 36:. doi: 10.1029/2009GL037245.

Rangwala I, Sinsky E, Miller JR (2016) Variability in projected elevation dependent warming in boreal midlatitude winter in CMIP5 climate models and its potential drivers. Clim Dyn 46:2115–2122. doi: 10.1007/s00382-015-2692-0.

Ruckstuhl C, Philipona R, Morland J, Ohmura A (2007) Observed relationship between surface specific humidity, integrated water vapor, and longwave downward radiation at different altitudes. J Geophys Res Atmos 112:. doi: 10.1029/2006JD007850.

Snyder M (2002) Climate responses to a doubling of atmospheric carbon dioxide for a climatically vulnerable region. Geophys Res Lett 29:9–12. doi: 10.1029/2001gl014431.

Sun B, Groisman PY, Bradley RS, Keimig FT (2000) Temporal Changes in the Observed Relationship between Cloud Cover and Surface Air Temperature. J Clim 13:4341–4357. doi: 10.1175/1520-0442(2000)013<4341:TCITOR>2.0.CO2.2.

Teichmann C, Eggert B, Elizalde A, Haensler A, Jacob D, Kumar P, Moseley C, Pfeifer S, Rechid D, Remedio AR, Ries H (2013) How does a regional climate model modify the projected climate change signal of the driving GCM: A study over different CORDEX regions using REMO. Atmosphere (Basel) 4:214–236. doi: 10.3390/atmos4020214.

Thompson, LG, Mosley-Thompson, E, Davis, ME, Lin, PN, Henderson, K and Mashiotta, TA (2003) Tropical glacier and ice core evidence of climate change on annual to millennial time scales. Clim Change 59:137–155. doi: 10.1023/A:1024472313775.

Van Vuuren DP, Eickhout B, Lucas PL, den Elzen MGJ (2006) Long-term multi-gas scenarios to stabilise radiative forcing - Exploring costs and benefits within an integrated assessment framework. Energy J 27:201–233. doi: 10.5547/ISSN0195-6574-EJ-VolSI2006-NoSI3-10.

Van Vuuren, DP, Edmonds, J, Kainuma, M, Riahi, K, Thomson, A, Hibbard, K, Hurtt, GC, Kram, T, Krey, V, Lamarque, JF, Masui, T (2011) The representative concentration pathways: An overview. Clim Change 109:5–31. doi: 10.1007/s10584-011-0148-z.

Xu J, Grumbine RE, Shrestha A, Eriksson M, Yang X, Wang YU, Wilkes A. (2009) The melting Himalayas: Cascading effects of climate change on water, biodiversity, and livelihoods. Conserv Biol 23:520–530. doi: 10.1111/j.1523-1739.2009.01237.x.

Yan, L., Liu, Z., Chen, G., Kutzbach, J. E., and Liu, X. (2016). Mechanisms of elevation-dependent warming over the Tibetan plateau in quadrupled CO 2 experiments. Climatic change, 135(3-4), 509-519. doi: 10.1007/s10584-016-1599-z.

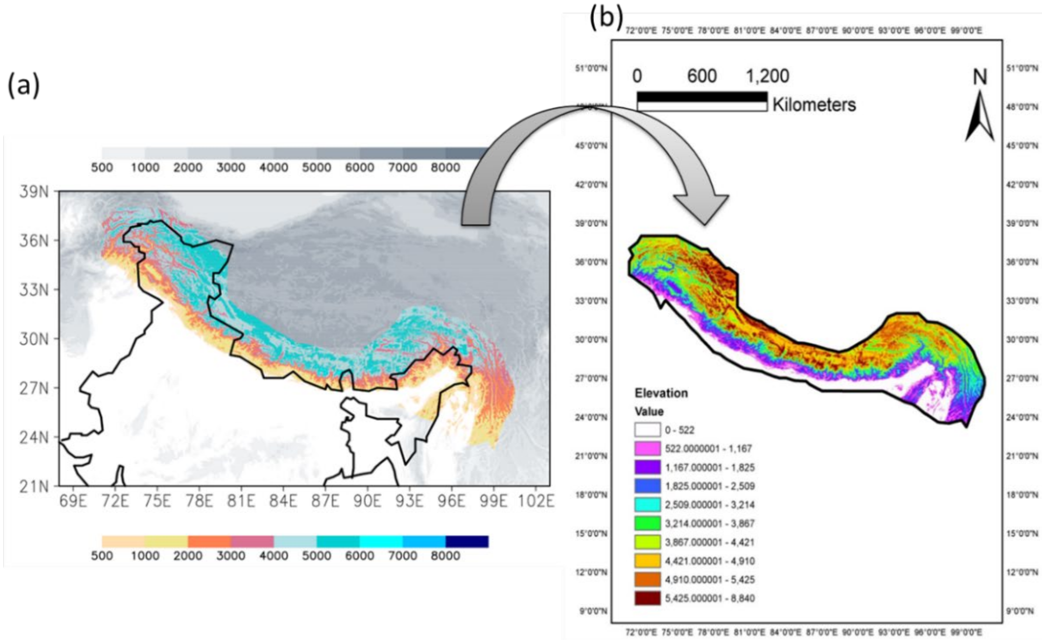

Fig. 1. Topography (m a.s.l.) of (a) the Himalayan-Tibetan Plateau region with (b) a focus on the area of this study (reproduced from Ghimire et al., 2015). This region is considered mainly over the southern rim of the Himalayas and is referred often in the text as Indian Himalayan Region (IHR) (Ghimire et al., 2015).

(a)

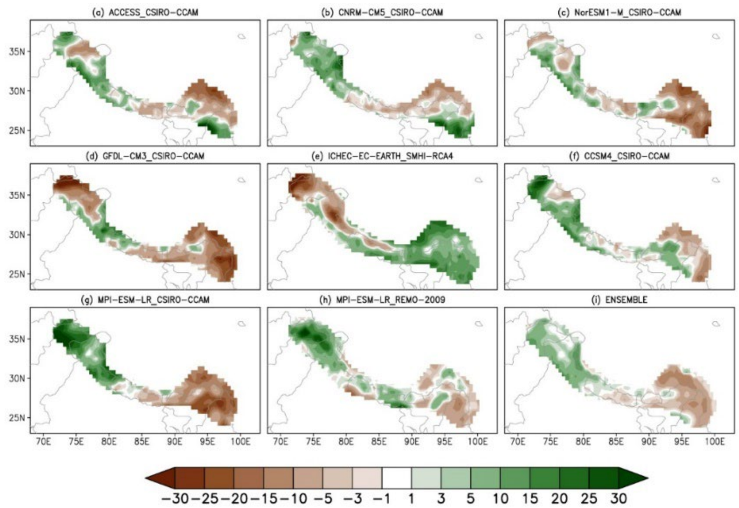

(b)

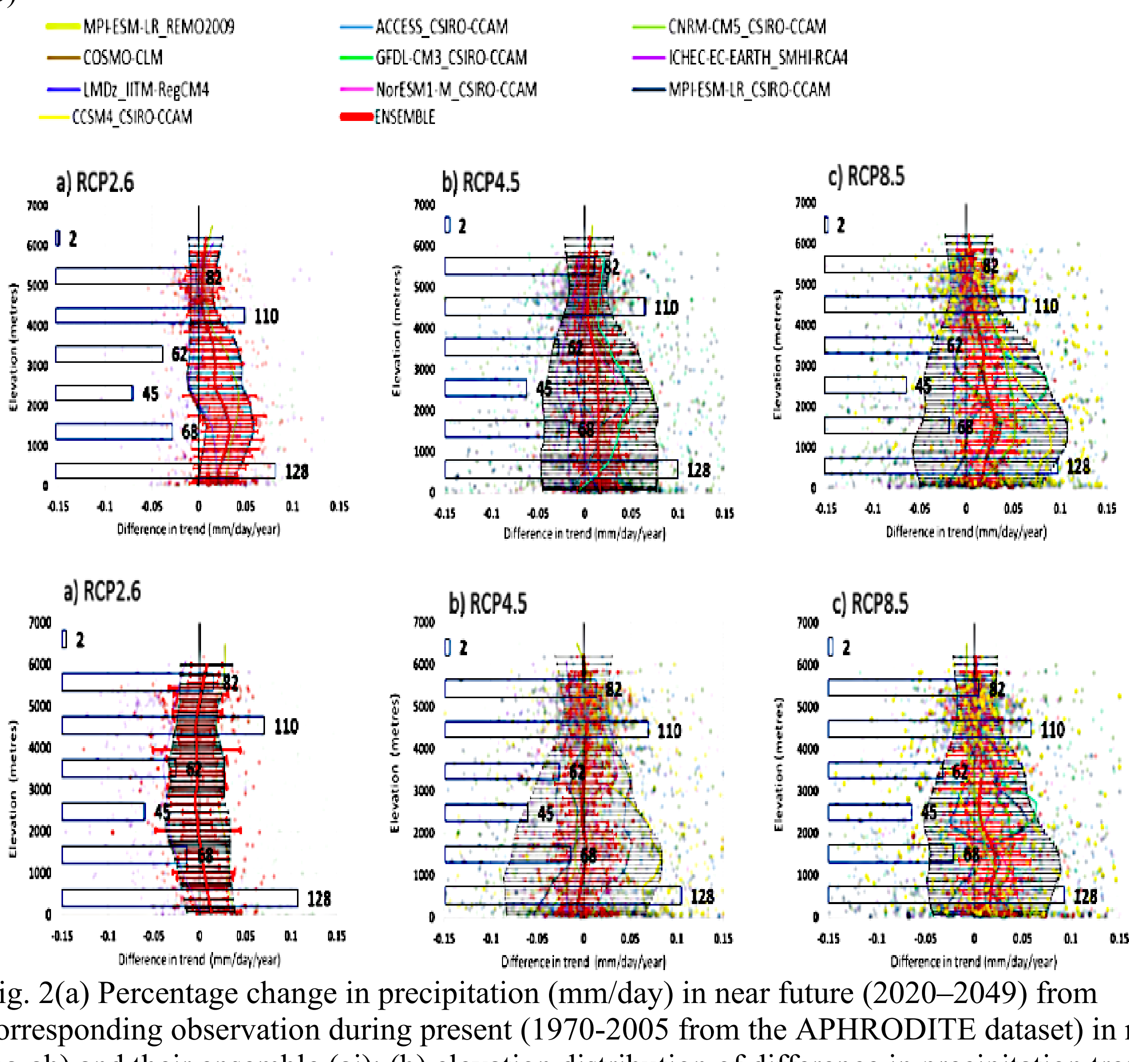

Fig. 2(a) Percentage change in precipitation (mm/day) in near future (2020–2049) from corresponding observation during present (1970-2005 from the APHRODITE dataset) in models (aa-ah) and their ensemble (ai); (b) elevation distribution of difference in precipitation trends (mm/day/year) in available models (scatter plots), errors (in bar) and their ensemble (red color line) in near future (2020–2049) from present (1970-2005 from the APHRODITE dataset) during winter (DJF, ba-bc) and monsoon (JJAS, bd-bf) in RCPs 2.6, 4.5 and 8.5 respectively.

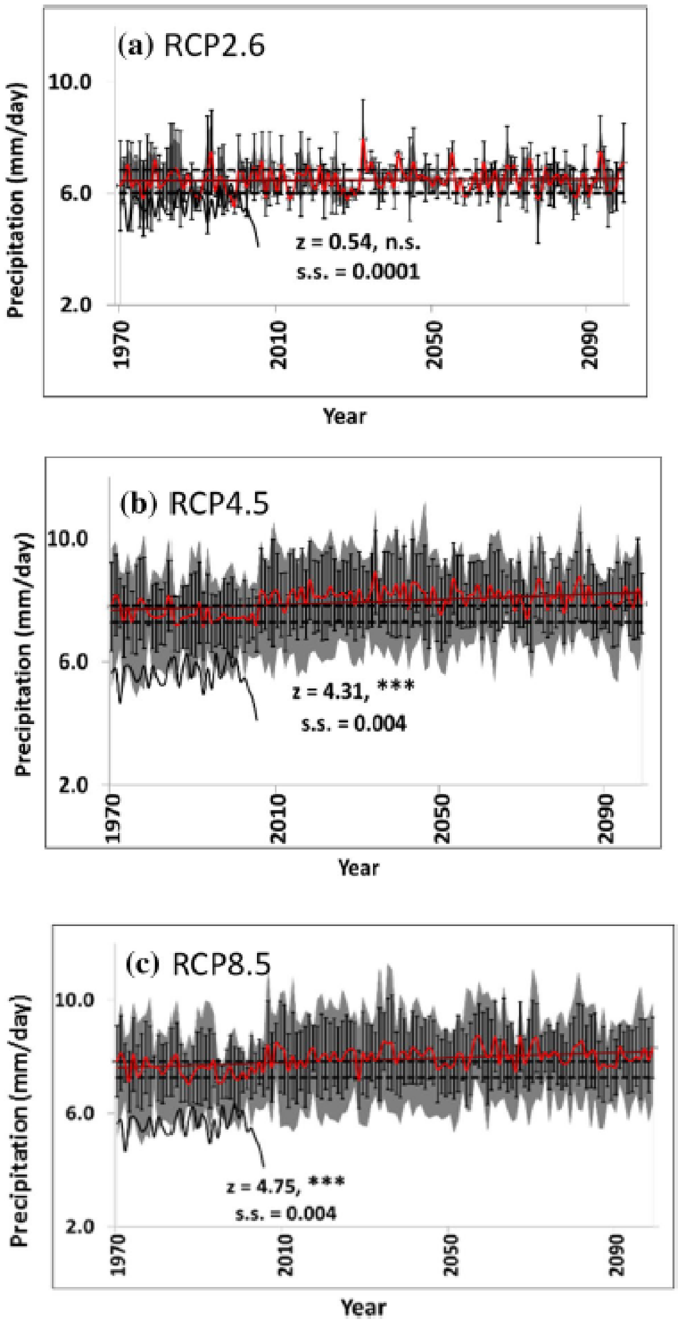

Fig. 3. Time series of JJAS mean precipitation (mm/day) for the 130 years (1970–2099) averaged over Himalayan region from ensemble of 2 CORDEX-SA experiments for (a) RCP2.6, 7 experiments for (b) RCP4.5 and 9 experiments for (c) RCP8.5. The *red line* represents the yearly values of JJAS mean precipitation. The *error bars* represent ensemble mean ± 1 standard deviation and the *grey shading* shows the minimum and maximum values over all ensemble members. Also shown are the yearly values of JJAS mean precipitation from observation APHRODITE (*black*) for 1970–2005 to indicate wet bias inherent in the models. *Brown straight*

line represents the linear trend (as Theil-Sen slope) in seasonal mean precipitation. The *dashed horizontal black lines* represent ± one standard deviation from the mean of present climate period 1970–2005, which shows the range of baseline variability. ‘z’ is the Mann–Kendall statistic for test of significance of trend at α = 0.05 where n.s., ‘*’, ‘**’ and ‘***’ implies non-significant, poorly significant (P ≤ 0.05), moderately significant (P ≤ 0.01) and strongly significant (P ≤ 0.001) respectively. ‘s.s’ is the Theil-Sen slope parameter (in units of mm/day/year).

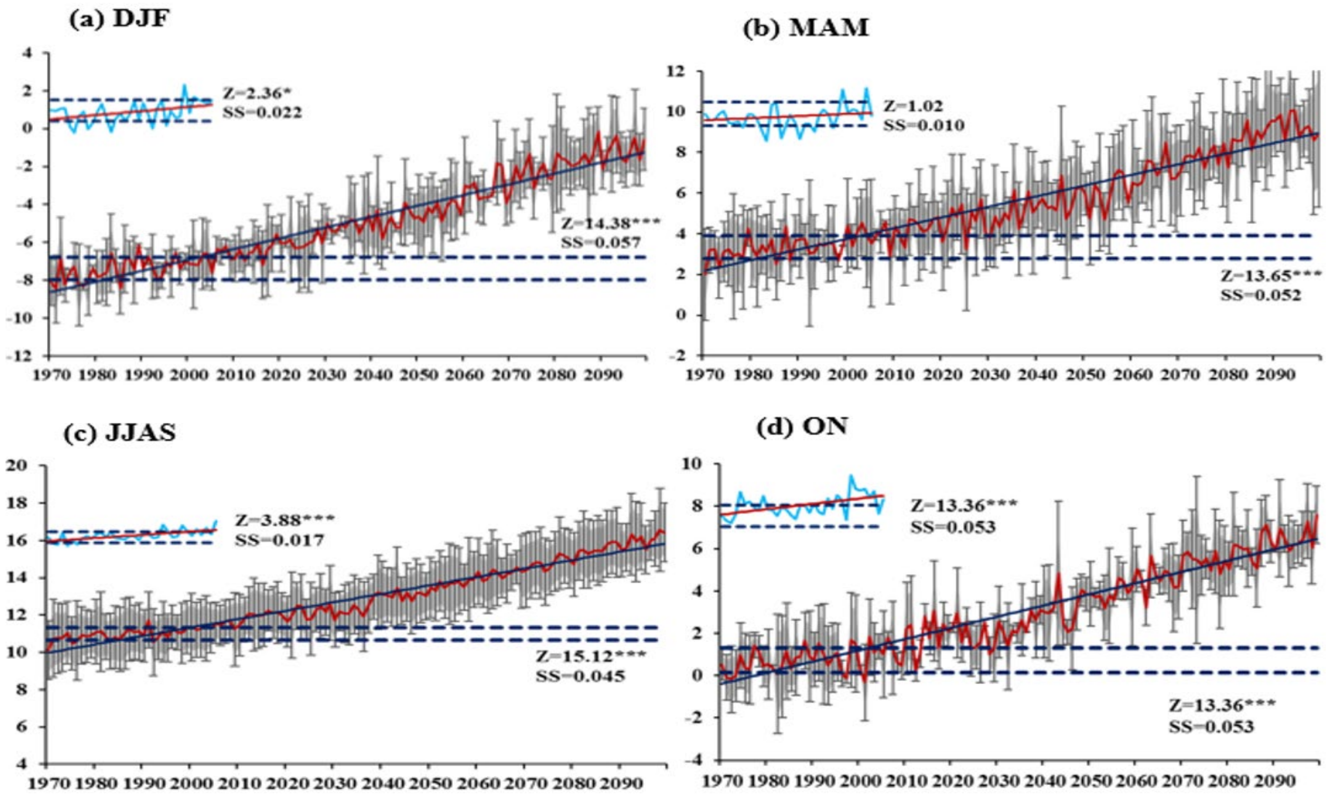

Fig. 4. Mean daily temperature (°C) for the 129-year period (1971-2099) averaged over Himalayan region from ensembles of CORDEX-SA under RCP8.5 for (a) DJF, (b) MAM, (c) JJAS and (d) ON seasons. Red line represents the yearly values of the ensemble, the error bars represent ensemble mean ± standard deviation and the grey shading shows the minimum and maximum values over all ensemble members. The yearly values of present observation (1970-2005 from the APHROTEMP dataset) are shown in light blue with dark blue representing mean ± standard deviation. Solid navy blue line represents the linear trend (as Theil-Sen slope) in seasonal mean temperature. The dashed horizontal black lines represent mean ± one standard deviation for each experiment and their ensemble for the present climate period 1970-2005, which shows the range of baseline variability. ‘z’ is the Man-Kendall statistic for test of significance of trend at α=0.05 where ‘no star’, ‘*’, ‘**’ and ‘***’ implies non-significant, poorly significant (P ≤ 0.05), moderately significant (P ≤ 0.01) and strongly significant (P ≤ 0.001) respectively. ‘SS’ is the Theil-Sen slope parameter.

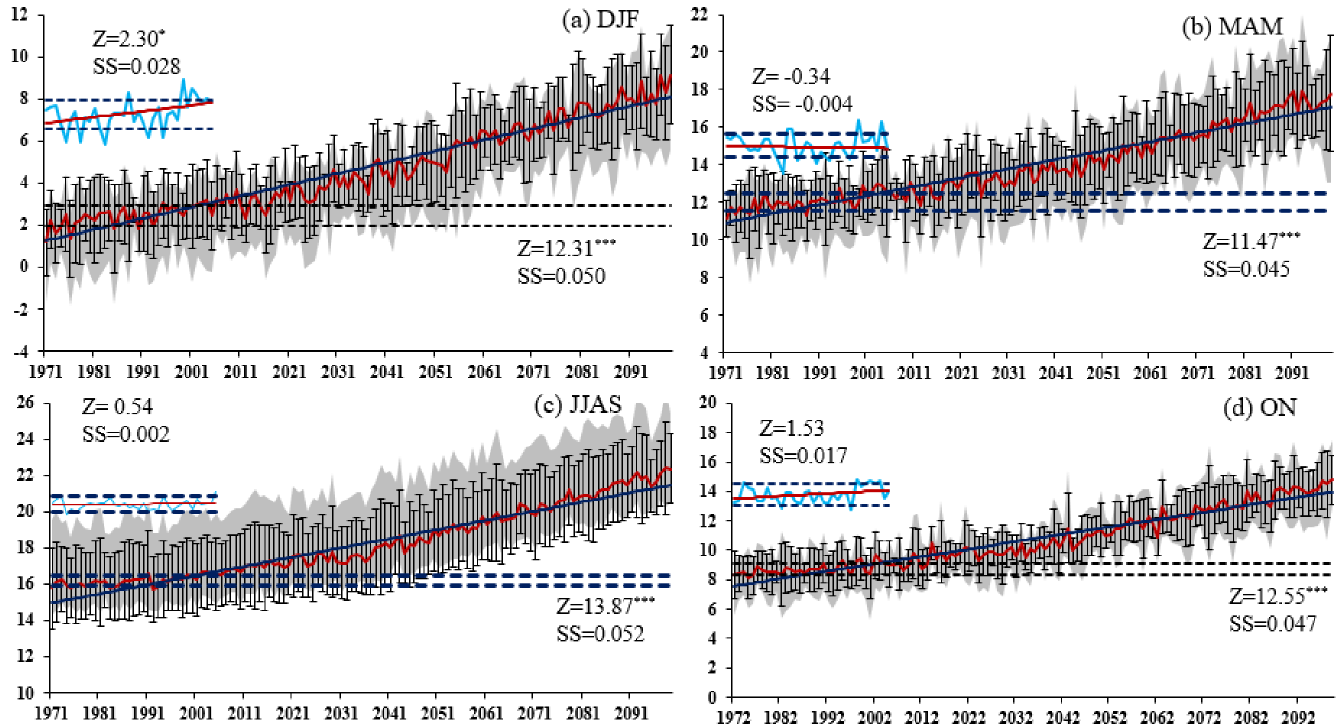

Fig. 5. Same as Fig. 4, but for maximum temperature (°C)

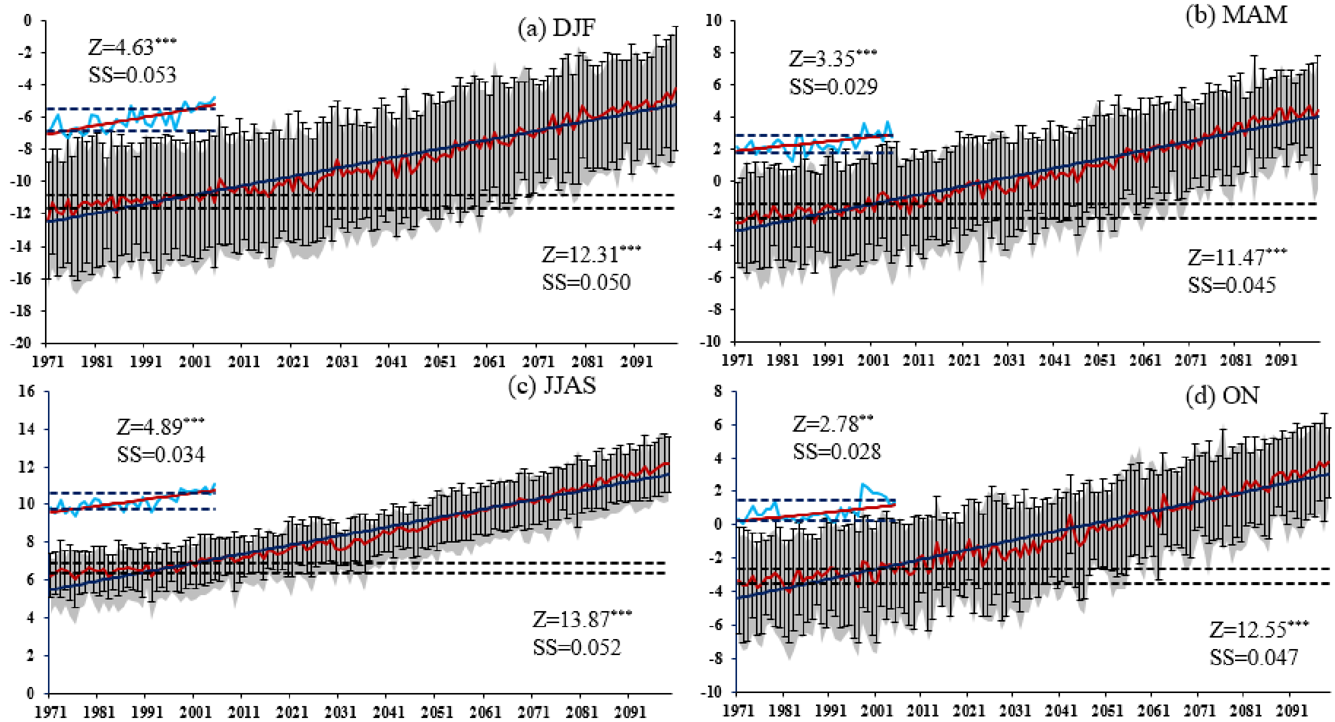

Fig. 6. Same as Fig. 4, but for minimum temperature (°C)

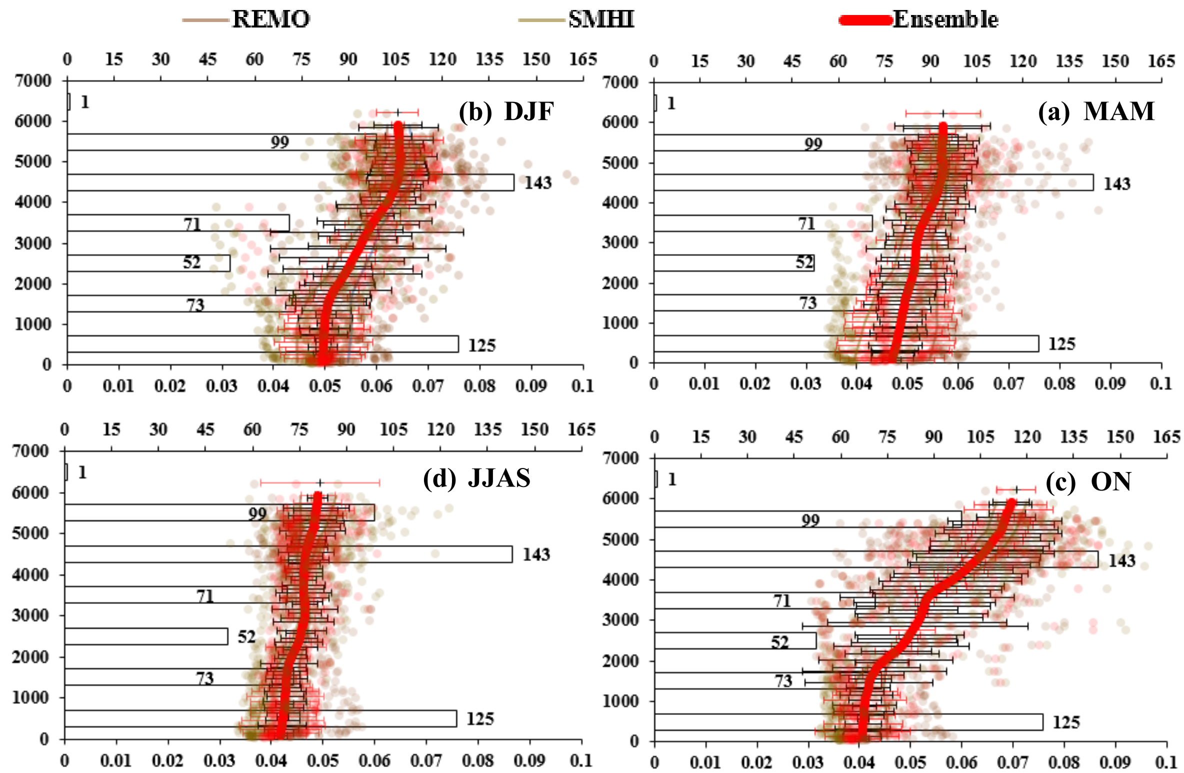

Fig. 7. Elevation distribution of difference in temperature trends (ºC/year) in near future (2020–2049) from present (1970-2005) during winter (DJF, a), pre-monsoon (MAM, b), monsoon (JJAS, c) and post- monsoon (d) in two best suited RCMs (REMO and SMHI) model (error bars) and ensemble (red line). Model simulations are carried out for 1970 – 2099 and present (1970-2005 from the APHROTEMP dataset).The thick colored line in each panel is obtained by averaging the trend values (scatted colored circles) within 1000 m-thick elevational bins and applying a smoothing procedure. The error bar in each plot shows the spatial variability within each 1000 m-thick elevational bins, while the rectangular bars with numbers indicate the number of grid points within each 1000 m-thick elevational bins (0-1000 m, 1000-2000 m, and so on).

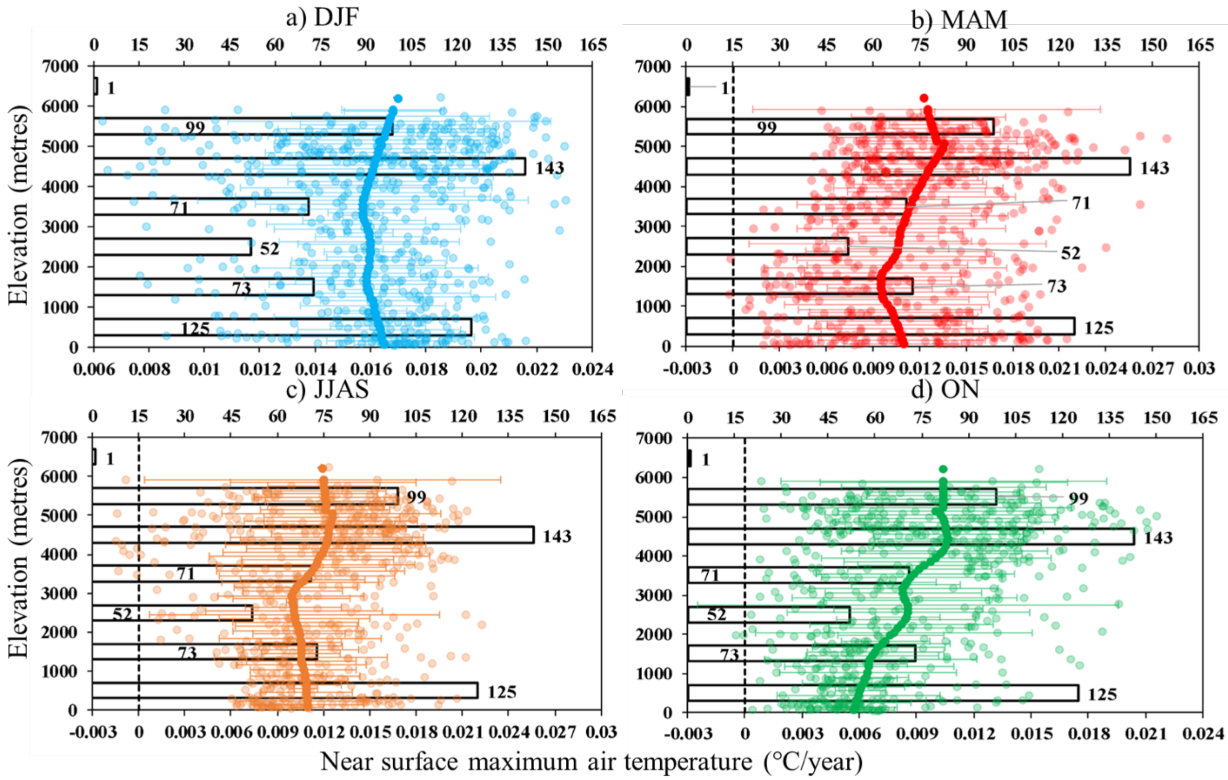

Fig. 8. Trends over the model simulation period 1970-2099 of the maximum temperature as a function of elevation (°C/year) during the (a) winter, (b) pre-monsoon, (c) monsoon and (d) post-monsoon seasons from REMO simulations under the RCP2.6 scenario. The thick colored line in each panel is obtained by averaging the trend values (scatted colored circles) within 1000 m-thick elevational bins and applying a smoothing procedure. The error bar in each plot shows the spatial variability within each 1000 m-thick elevational bins, while the rectangular bars with numbers indicate the number of grid points within each 1000 m-thick elevational bins (0-1000 m, 1000-2000 m, and so on).

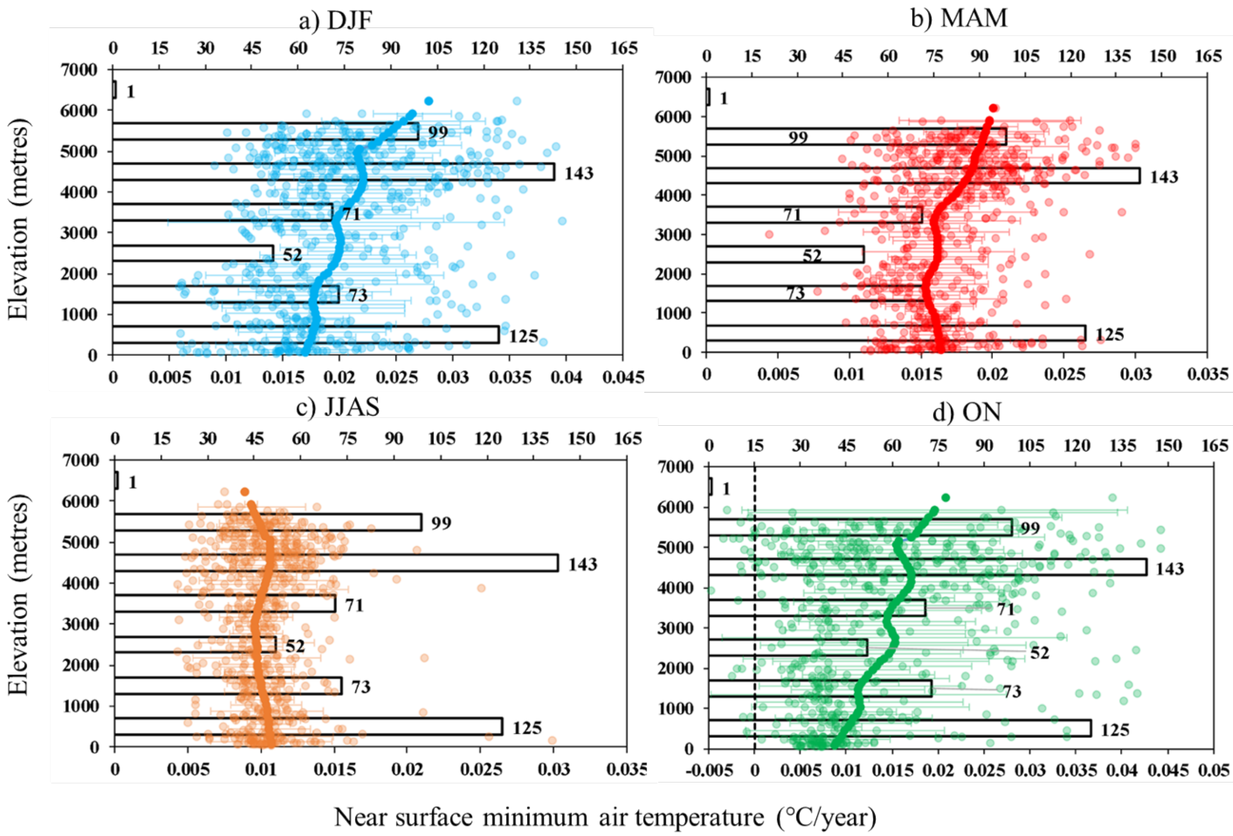

Fig. 9. Same as Fig. 8, but for minimum temperature (°C/year).

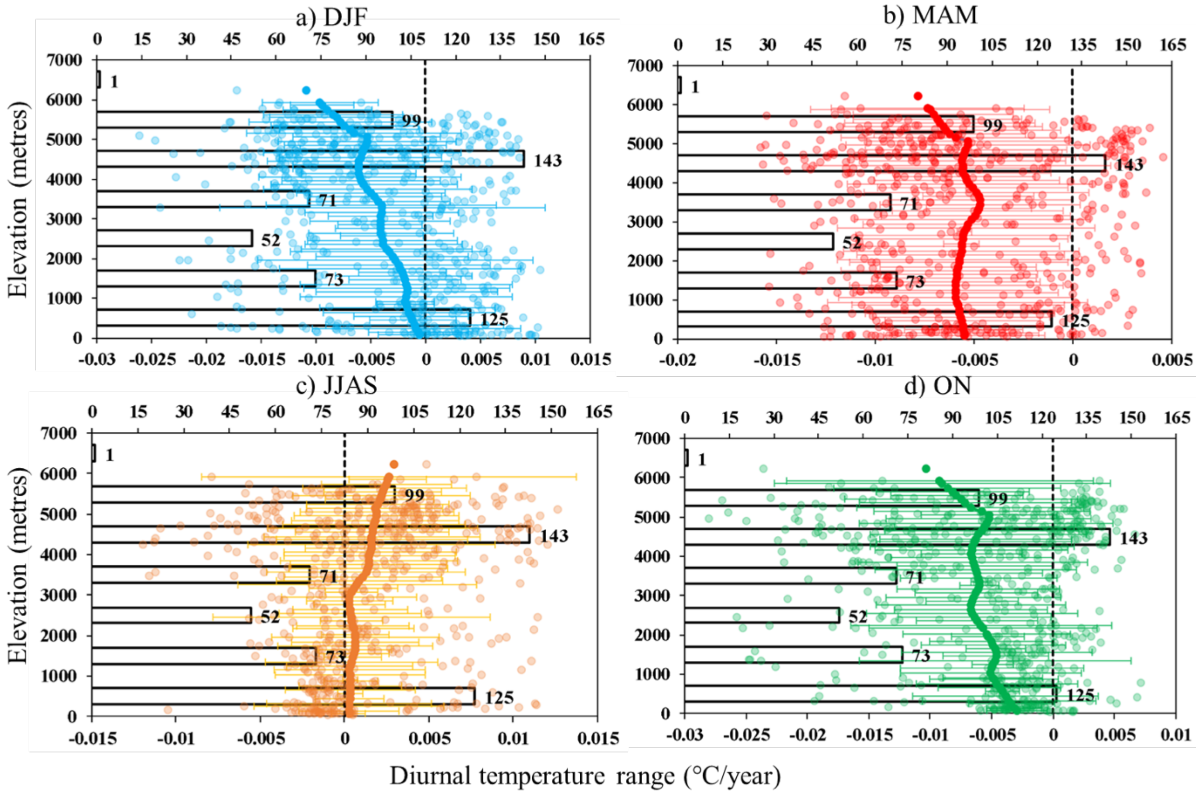

Fig. 10. Same as Fig. 8, but for Diurnal Temperature Range (°C/year).

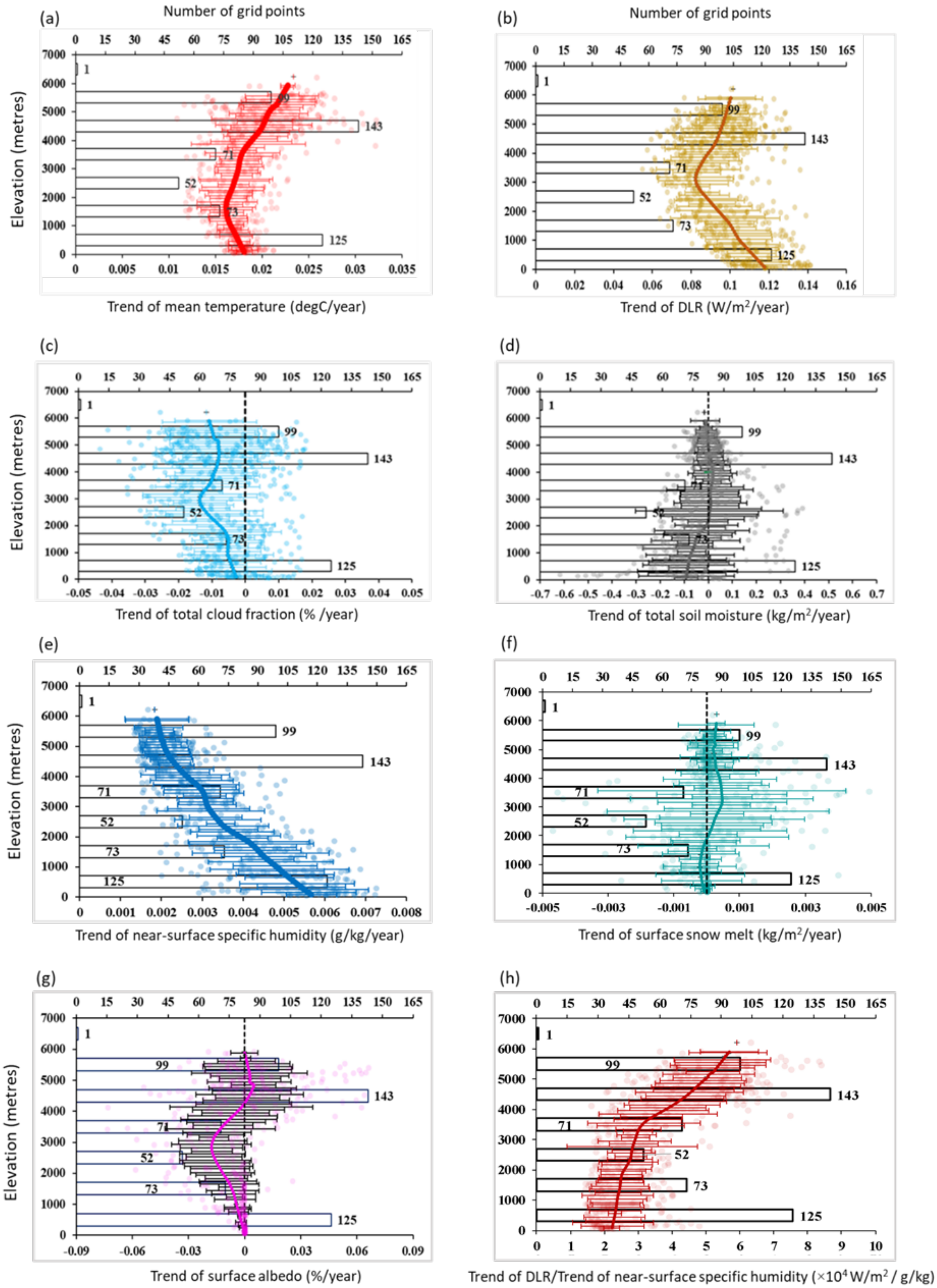

Fig.11. Elevation dependent trends (trends are evaluated over the period 1970-2099, the RCP2.6 scenario is considered in the projection period 2006-2099) of (a) mean temperature (°C/year) (b) downwelling longwave radiation (W/m^2/year), (c) total cloud fraction (%/year), (d) total soil moisture (kg/m^2/year), (e) specific humidity (g/kg/year), (f) surface snow melt (kg/m^2/year), (g)

surface albedo (%/year) and (h) ratio of the DLR trend and near-surface specific humidity trend ($\times 10^4$ W/m^2/g/kg), during the winter season. The thick colored line in each panel is obtained by averaging the trend values (scattered colored circles) within 1000 m-thick elevational bins and applying a smoothing procedure. The error bar in each plot shows the spatial variability within each 1000 m-thick elevational bins, while the rectangular bars with numbers indicate the number of grid points within each 1000 m-thick elevational bins (0-1000 m, 1000-2000 m, and so on) (source: Himalayan Weather and Climate and their Impact on the Environment, eds. Dimri et al. ISBN 978-3-030-29683-4, © Springer Nature Switzerland AG 2020).

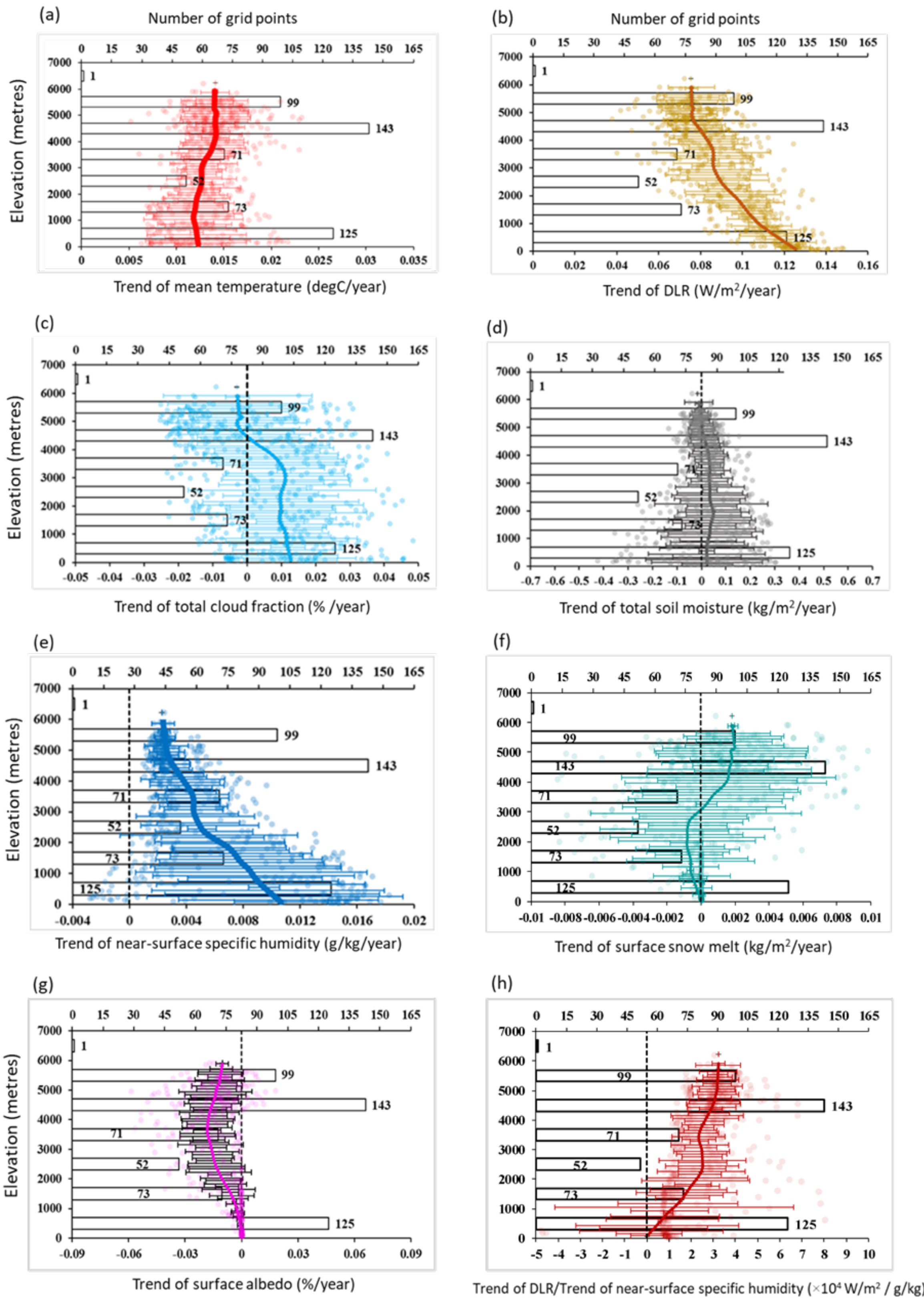

Fig. 12. Same as Fig. 11, but for the pre-monsoon season.

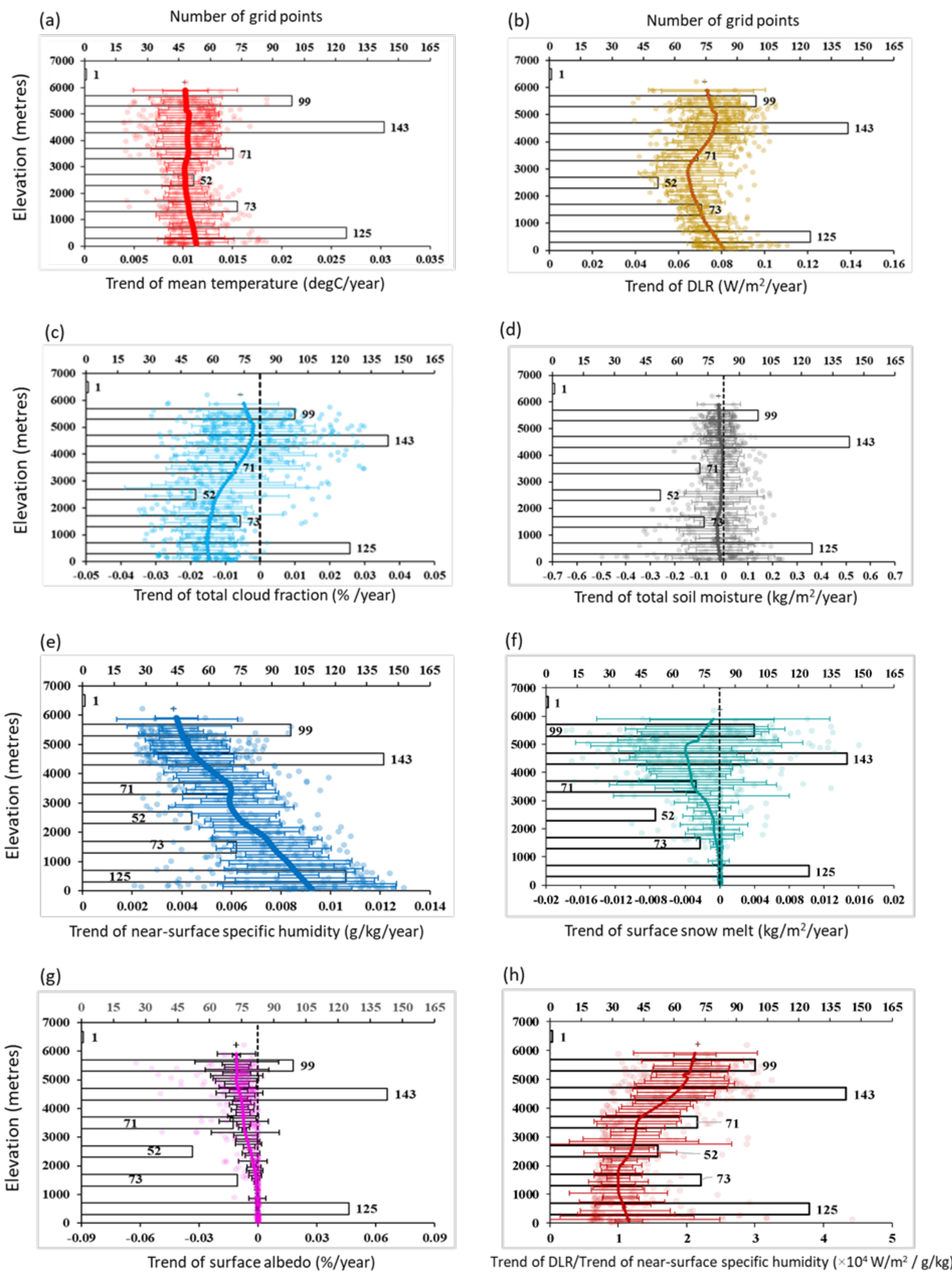

Fig. 13. Same as Fig. 11, but for the monsoon season.

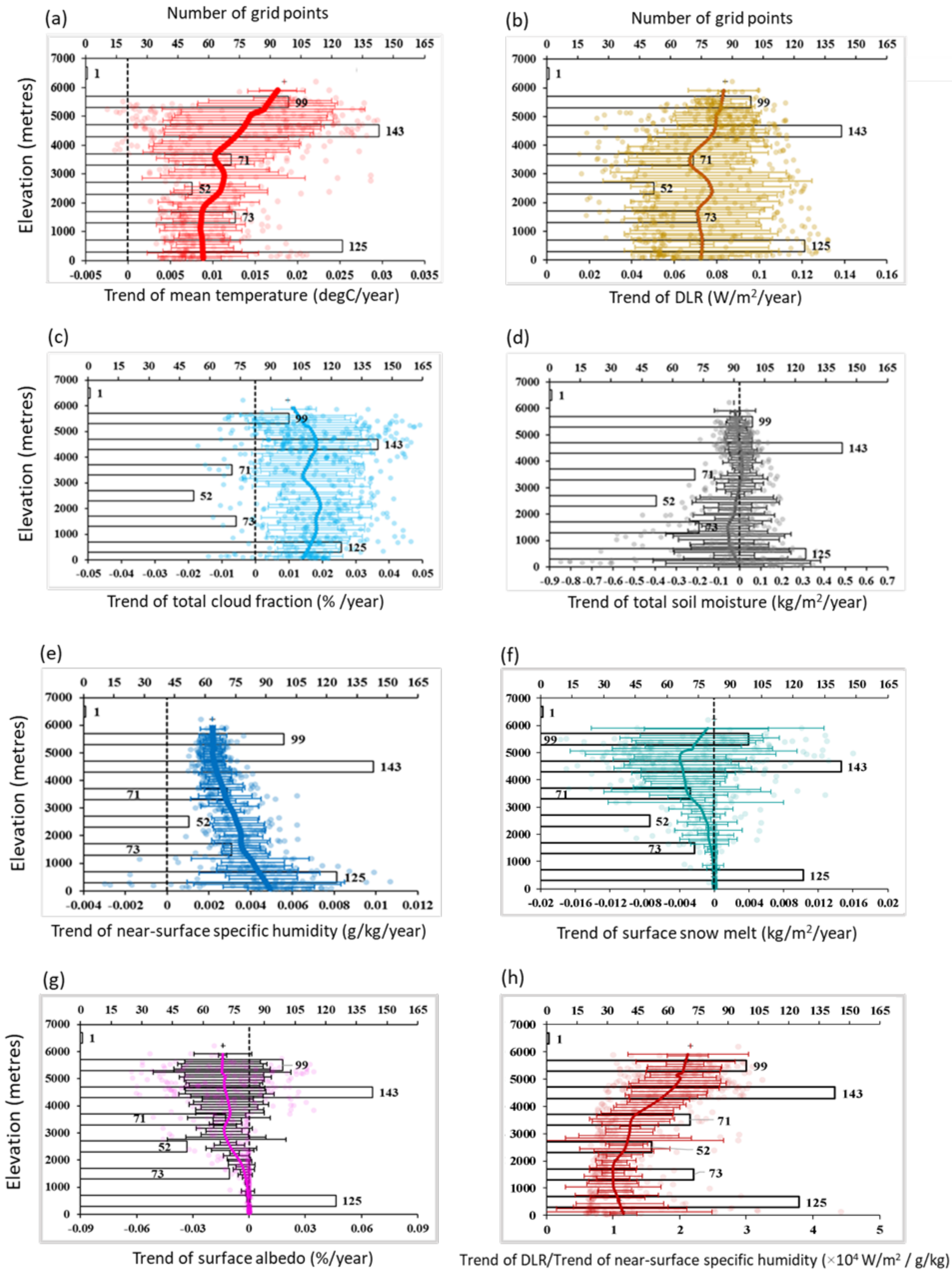

Fig. 14. Same as Fig. 11, but for the post-monsoon season.

(a)

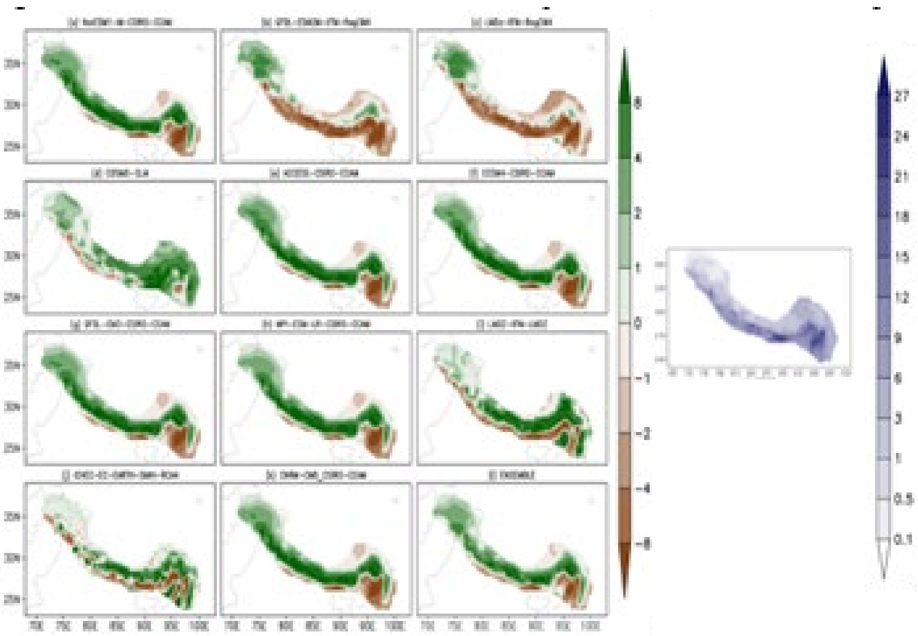

(b)

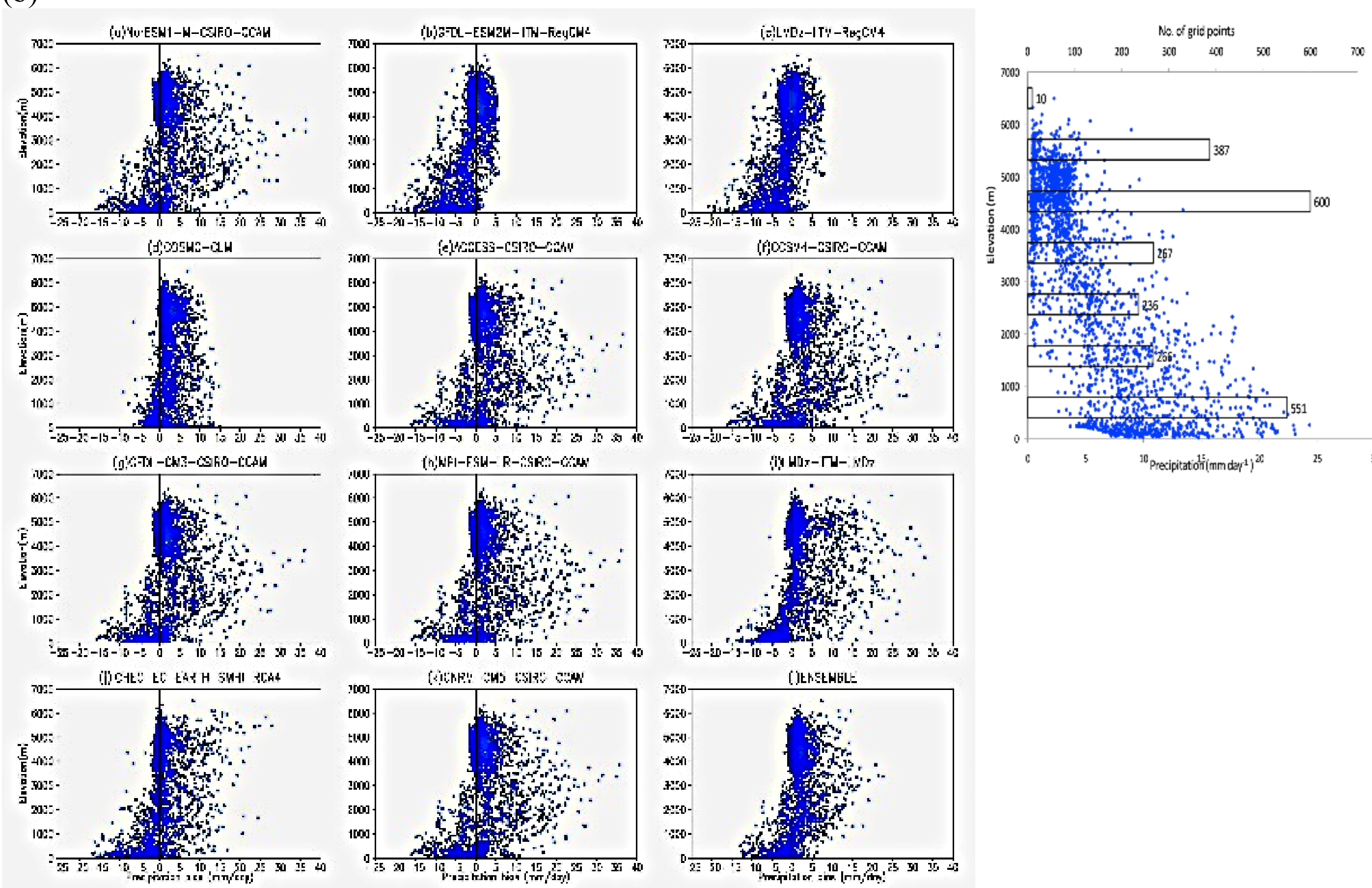
(d)COSMO-CLM
(l)ENSEMBLE
No. of grid points
Elevation (m)
Precipitation (mm day-1)

(c)

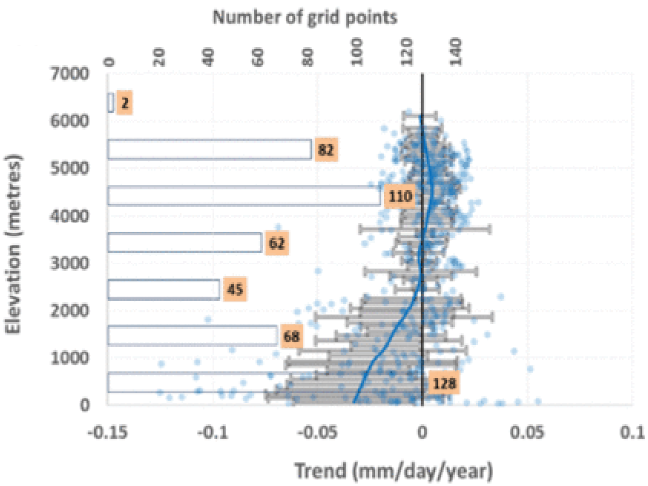

Fig. S1(a) Spatial distribution of mean monsoon (JJAS) precipitation (mm/day, right hand panel) and models (aa -ak) and their ensemble (al) biases from the corresponding observation (left hand panels) during present (1970-2005 from the APHRODITE dataset); (b) elevation scatter grid distribution of annual averaged precipitation (mm/day, right hand panel) and model (ba-bk) and their ensemble (bl) differences from the corresponding observation (left hand panels) during present (1970-2005 from the APHRODITE dataset); (c) precipitation trend (mm/day/year) as a function of the elevation during the period 1970-2005 (from the APHRODITE dataset). The thick colored line in (c) is obtained by averaging the temperature trend values (blue empty circles) within 1000m elevational bins and applying a smoothing procedure. The error bar in (c) shows the spatial variability within each 1000m thick bin. The bars with numbers indicate the number of grid points falling within each 1000m altitude range (Source for Fig. a and b: Ghimire et al., 2015).

(a)

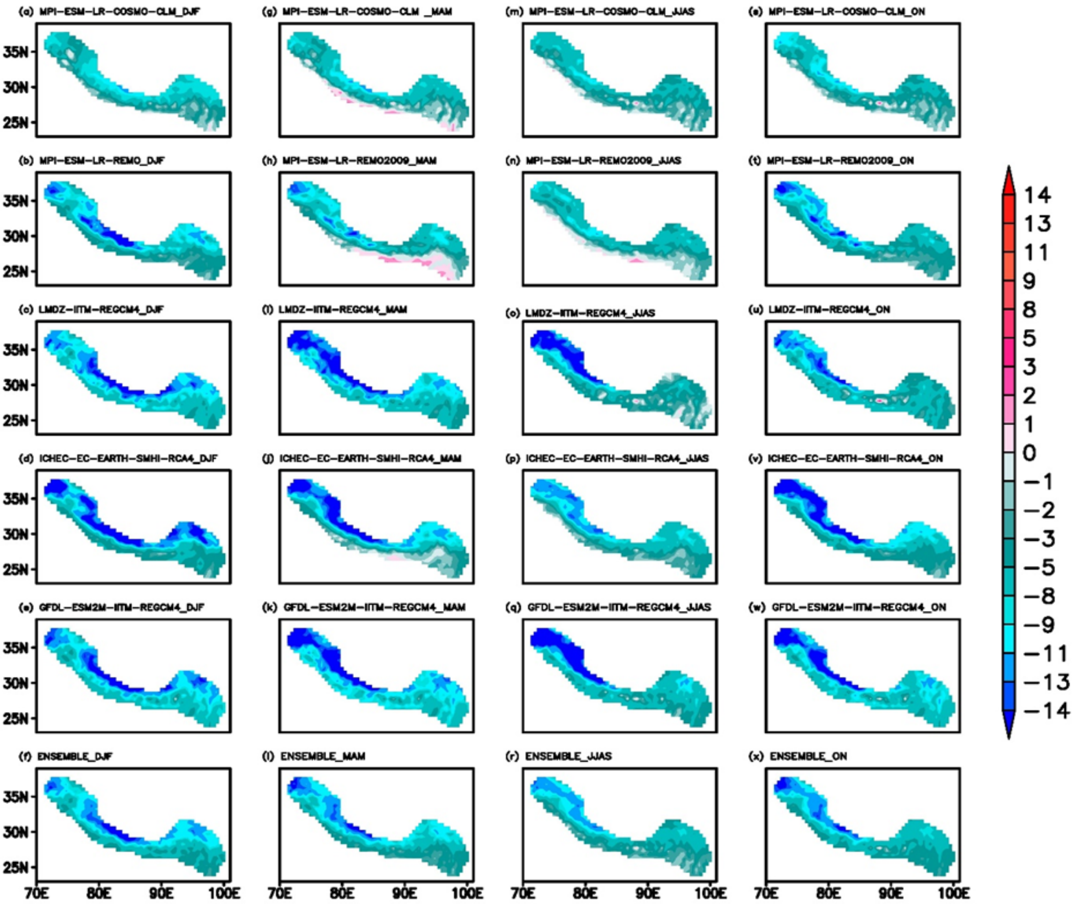

(a) MPI-ESM-LR-COSMO-CLM_DJF
(g) MPI-ESM-LR-COSMO-CLM _MAM
(m) MPI-ESM-LR-COSMO-CLM_JJAS
(s) MPI-ESM-LR-COSMO-CLM_ON
(b) MPI-ESM-LR-REMO_DJF
(h) MPI-ESM-LR-REMO2009_MAM
(n) MPI-ESM-LR-REMO2009_JJAS
(t) MPI-ESM-LR-REMO2009_ON
(c) LMDZ-IITM-REGCM4_DJF
(i) LMDZ-IITM-REGCM4_MAM
(o) LMDZ-IITM-REGCM4_JJAS
(u) LMDZ-IITM-REGCM4_ON
(d) ICHEC-EC-EARTH-SMHI-RCA4_DJF
(j) ICHEC-EC-EARTH-SMHI-RCA4_MAM
(p) ICHEC-EC-EARTH-SMHI-RCA4_JJAS
(v) ICHEC-EC-EARTH-SMHI-RCA4_ON
(e) GFDL-ESM2M-IITM-REGCM4_DJF
(k) GFDL-ESM2M-IITM-REGCM4_MAM
(q) GFDL-ESM2M-IITM-REGCM4_JJAS
(w) GFDL-ESM2M-IITM-REGCM4_ON
(f) ENSEMBLE_DJF
(l) ENSEMBLE_MAM
(r) ENSEMBLE_JJAS
(x) ENSEMBLE_ON
35N
30N
25N
70E
80E
90E
100E
14
13
11
9
8
5
3
2
1
0
−1
−2
−3
−5
−8
−9
−11
−13
−14

(b)

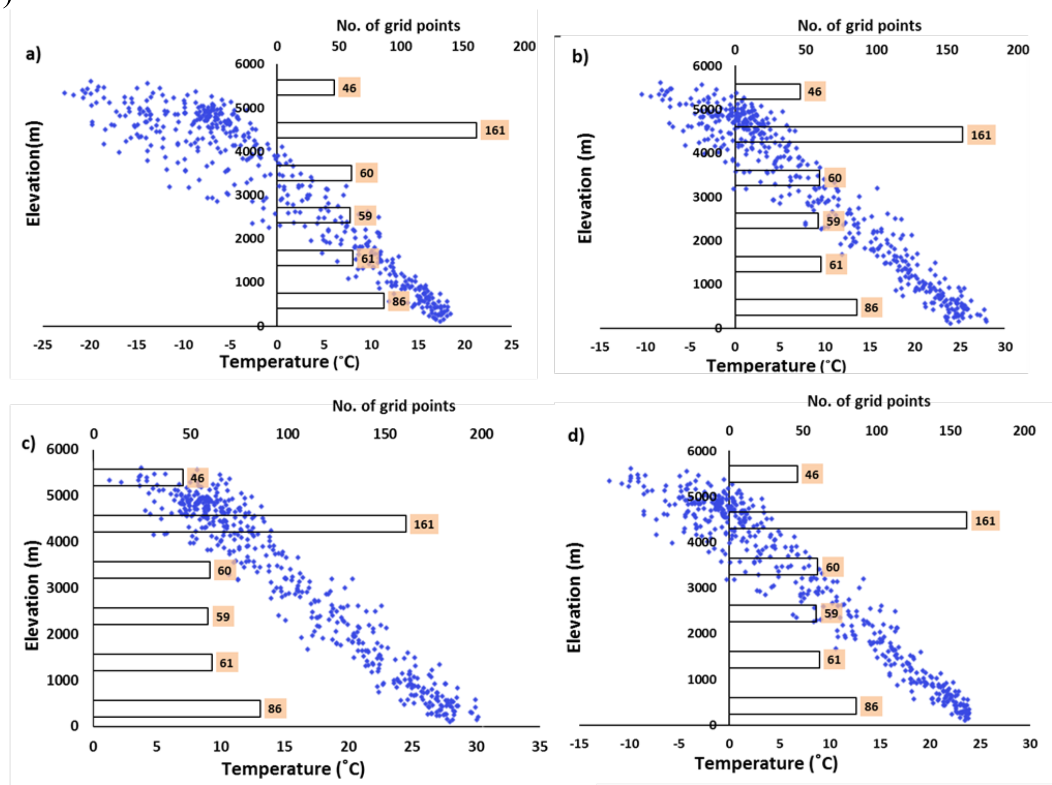

a)
b)
c)
d)
No. of grid points
Elevation (m)
Temperature (˚C)
46
161
60
59
61
86

(c)

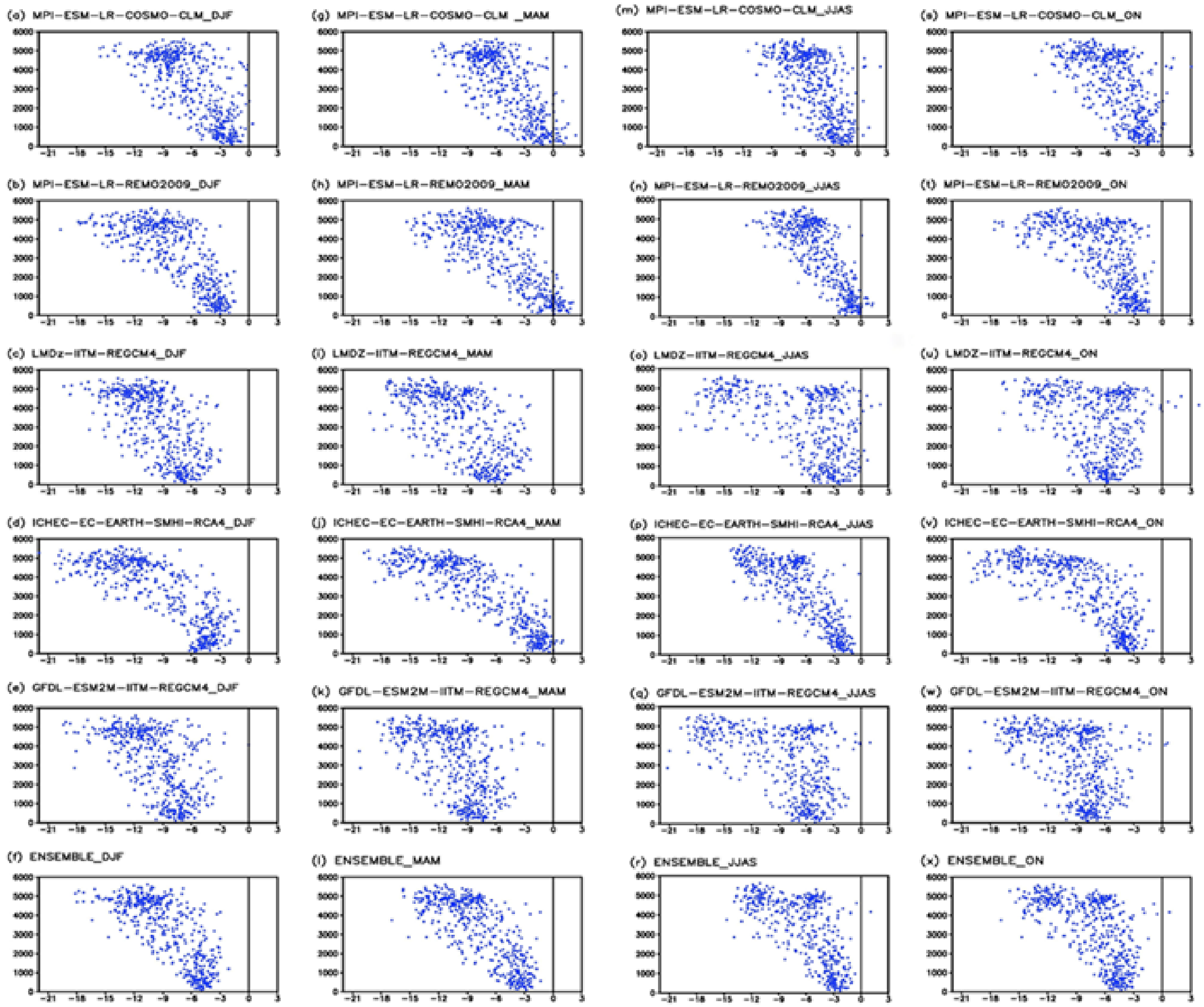
(a) MPI-ESM-LR-COSMO-CLM_DJF
(g) MPI-ESM-LR-COSMO-CLM _MAM
(m) MPI-ESM-LR-COSMO-CLM_JJAS
(s) MPI-ESM-LR-COSMO-CLM_ON
(b) MPI-ESM-LR-REMO2009_DJF
(h) MPI-ESM-LR-REMO2009_MAM
(n) MPI-ESM-LR-REMO2009_JJAS
(t) MPI-ESM-LR-REMO2009_ON
(c) LMDz-IITM-REGCM4_DJF
(i) LMDZ-IITM-REGCM4_MAM
(o) LMDZ-IITM-REGCM4_JJAS
(u) LMDZ-IITM-REGCM4_ON
(d) ICHEC-EC-EARTH-SMHI-RCA4_DJF
(j) ICHEC-EC-EARTH-SMHI-RCA4_MAM
(p) ICHEC-EC-EARTH-SMHI-RCA4_JJAS
(v) ICHEC-EC-EARTH-SMHI-RCA4_ON
(e) GFDL-ESM2M-IITM-REGCM4_DJF
(k) GFDL-ESM2M-IITM-REGCM4_MAM
(q) GFDL-ESM2M-IITM-REGCM4_JJAS
(w) GFDL-ESM2M-IITM-REGCM4_ON
(f) ENSEMBLE_DJF
(l) ENSEMBLE_MAM
(r) ENSEMBLE_JJAS
(x) ENSEMBLE_ON

(d)

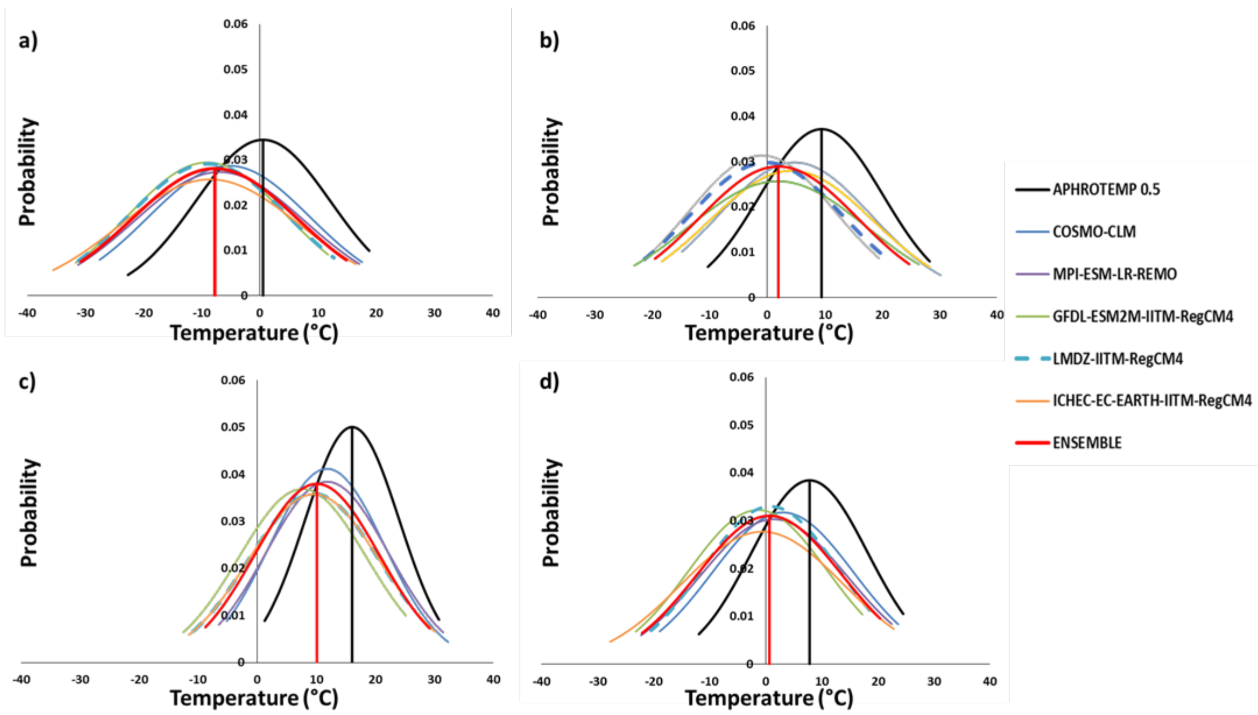
a)
b)
c)
d)
Probability
Temperature (°C)
APHROTEMP 0.5
COSMO-CLM
MPI-ESM-LR-REMO
GFDL-ESM2M-IITM-RegCM4
LMDZ-IITM-RegCM4
ICHEC-EC-EARTH-IITM-RegCM4
ENSEMBLE

Fig. S2(a) Spatial distribution of mean winter (DJF, left most panel), pre-monsoon (MAM, middle left panel), monsoon (JJAS, middle right panel) and post-monsoon (ON, right most panel) temperature biases (ºC/day) with available models and their ensemble during present (1970-2005 from the APHROTEMP dataset); (b) elevation dependent scatter grid distribution of averaged temperature (ºC) during winter (DJF, ba), pre-monsoon (MAM, bb), monsoon (JJAS, bc) and post-monsoon (ON, bd) during present (1970-2005 from the APHROTEMP dataset); (c) elevation dependent distribution of difference of mean winter (DJF, left most panel), pre-monsoon (MAM, middle left panel), monsoon (JJAS, middle right panel) and post-monsoon (ON, right most panel) temperature (ºC) during near future (2020–2049) from present (1970-2005 from the APHROTEMP dataset) in available models and their ensemble; (d) comparison of probability density function during present (1970-2005) from available models, their ensemble and the corresponding observation (APHROTEMP) during winter (DJF, da), pre-monsoon (MAM, db), monsoon (JJAS, dc) and post-monsoon (ON, dd) (Source: Nengker et al., 2017).